The University of Manitoba

Numerical Simulation of 2D Flow Past a Dimpled Cylinder Using a Pseudospectral Method

by

Marina Kotovshchikova

A thesis
submitted to the Faculty of Graduate Studies
of the University of Manitoba
in partial fulfillment of the requirements for the
degree of M. Sc. in Mathematics

Winnipeg, Manitoba, Canada, 2006

Abstract

A numerical simulation of steady and unsteady two-dimensional flows past cylinder with dimples based on highly accurate pseudospectral method is the subject of the present thesis. The vorticity-streamfunction formulation of two-dimensional incompressible Navier-Stokes equations with no-slip boundary conditions is used. The system is formulated on a unit disk using curvilinear body fitted coordinate system. Key issues of the curvilinear coordinate transformation are discussed, to show its importance in properly defined node distribution. For the space discretization of the governing system the Fourier-Chebyshev pseudospectral approximation on a unit disk is implemented. To handle the singularity at the pole of the unit disk the approach of defining the computational grid proposed by Fornberg was implemented. Two algorithms for solving steady and unsteady problems are presented. For steady flow simulations the non-linear time-independent Navier-Stokes problem is solved using the Newton's method. For the time-dependent problem the semi-implicit third order Adams-Bashforth/Backward Differentiation scheme is used. In both algorithms the fully coupled system with two no-slip boundary conditions is solved. Finally numerical result for both steady and unsteady solvers are presented. A comparison of results for the smooth cylinder with those from other authors shows good agreement. Spectral accuracy is demonstrated using the steady solver.

Acknowledgments

I wish to thank my supervisor Dr. S. H. Lui for his guidance and careful comments in the preparation of this thesis. Thanks for teaching me spectral methods and also for the topic and all the materials which helped me in this work.

I would like to acknowledge Professors Abba Gumel, Kirill Kopotun and Parimala Thulasiraman for teaching me many things and being part of my thesis committee. Thank you for your interest in my research, your time and all advises which helped me to improve the final copy of my thesis.

I also would like to acknowledge the financial support given to me by my supervisor, government of Manitoba, Faculty of Science of the University of Manitoba and UMSU (University of Manitoba Student Union). I am very thankful for all the support, without it this work wouldn't be possible.

And the last but not the least I would like to express my thanks to my husband Dr. Dmitry K. Firsov for his patience and support and for valuable advises in mathematics.

Table of Contents

List of Tables

List of Figures

Table of notations

u	velocity component on x axis
v	velocity component on y axis
$\mathbf{u}$	velocity vector
p	pressure
t	time
Re	Reynolds number, defines flow regime
∇	gradient operator
Δ	Laplacian $\Delta = \nabla^2$
μ	dynamic viscosity of a fluid
ρ	fluid density
U	characteristic velocity of the fluid flow(or a bluff body)
d	diameter of the circular cylinder
ω	vorticity
ψ	streamfunction
ϕ	new streamfunction $\phi = \psi - y$
$\lvert\cdot\rvert$	matrix determinant
$G(\omega, \psi)$, or $G(\omega, \phi)$	convective term of the Navier-Stokes system
$\gamma(\theta)$	parametric function of the dimpled surface
ϵ	depth of dimples
c	number of dimples
$\Gamma = (\Gamma_x, \Gamma_y)$	boundary
$\vec{n} = (n_x, n_y)$	outward normal vector on the boundary Γ
$\vec{\tau} = (\tau_x, \tau_y)$	tangent to the boundary Γ vector
Ω	semi-infinite physical domain with boundary Γ
E	unit disc, numerical domain
$f(R)$	map from $[0, 1]$ to $[1, \infty)$
J	Jacobian of the transformation $(R, \theta) \to (x, y)$
g	the matrix of the covariant metric tensor
g_{ij}	covariant metric tensor components
g^{ij}	contravariant metric tensor components
σ_w	shear stress on the solid wall
$\vec{F}$	net force acting on the surface of the body

$\vec{F}_{pressure}$	force due to pressure
$\vec{F}_{skin-friction}$	force due to shear stresses
F_D	drag force, x component of the net force $\vec{F}$
F_L	lift force, y component of the net force $\vec{F}$
C_D	dimensionless drag coefficient
C_L	dimensionless lift coefficient
L	differential operator $-\Delta$ and its pseudospectral approximation
E_{nM}	discrete unit disk
R_j	Chebyshev collocation point in the radial direction on E_{nM}
θ_k	Fourier collocation point in the angular direction on E_{nM}
n	the number of inner point in R direction in E_{nM}
M	the number of points in θ direction in E_{nM}
D, $D^{(2)}$	1st and 2nd order Chebyshev differential matrices
DF, $DF^{(2)}$	1st and 2nd order Fourier differential matrices
D_R	pseudospectral differential matrix of the $\partial/\partial R$ on E_{nM}
D_θ	pseudospectral differential matrix of the $\partial/\partial\theta$ on E_{nM}
$\otimes$	matrix tensor product operator
F	the residual in the Newton's method
J_F	the Jacobian of F
$\|\cdot\|_2$	the norm in L_2 space
Δt	discrete time step
r_j	the radial component of a point on the physical domain Ω
θ_s	angle position of the separation point of the wake on Γ
L_w	wake length along the x axis
St	Strouhal number, denotes dimensionless frequency

Chapter 1

Introduction

Problems that involve fluid (liquid or gas) flows arise from many science and engineering applications including design of vehicles and other technical devices, sport aero- and hydrodynamics etc. The motion of any fluid is described by the Navier-Stokes equations, hence these equations play the key role in any fluid dynamic simulations (`http://www.navier-stokes.net/`). The system of Navier-Stokes equations can be solved analytically only in some simple cases. In general Navier-Stokes equations are solved numerically by approximating the solution at finitely many points using a numerical method and solving the resulting linear system of equations on a computer. Development of numerical methods with high order of approximation and geometrical flexibility are of main interest in many of todays researches.

This project is devoted to the numerical simulation of the laminar viscous fluid flow past a cylindrical body with dimples. The numerical method is based on the application of the Fourier-Chebyshev pseudospectral (spectral collocation) method. Spectral methods are known for giving highly accurate numerical solutions and in fluid mechanics they are usually applied for spatial discretization, while lower order methods are used for time schemes. In this project we focus on the high order approximations in space and use 2-4 order finite difference methods for time integration. One of the reasons for this project is an application of pseudospectral simulation to the flow in complex geometry and obtaining solution with spectral accuracy. By experimenting with geometry (number and size of dimples on the cylinder) we study

how flow characteristics are changed.

1.1 External flow problems

External flow problems arise from many engineering and science applications: flow past electrical wires, sport balls, vehicles etc. The control of the flow over a bluff body for drag reduction is one of the major issues in fluid mechanics. Flows over a cylinder (2-dimensional bluff body) and a sphere (3-dimensional bluff body) are two of the most studied bluff body problems. To control the flow past these bodies two distinct approaches are used: active, using external forcing [27], and passive, using shape modifications [1, 3, 32].

Bluff body problems are studied experimentally or by direct numerical simulations. Numerical simulations are based on the solution of the Navier-Stokes system of equations. In many applications the media can be considered as an incompressible viscous fluid and the Navier-Stokes system of equations, that describes its motion, includes the momentum equations:

$$\frac{\partial \mathbf{u}}{\partial t} + \nabla \mathbf{u} \cdot \mathbf{u} - \frac{1}{Re} \Delta \mathbf{u} = -\nabla p$$

and the equation of continuity (or equation of mass conservation):

$$\nabla \cdot \mathbf{u} = 0$$

Here $\mathbf{u}$ is a velocity vector, p-pressure, and Re is a Reynolds number defined by $Re = \rho La/\mu$, where L, a are the characteristic length and velocity of the fluid flow (or a bluff body) and ρ, μ are density and dynamic viscosity of the fluid. Reynolds number determines the flow regime. For instance the flow past a cylinder at low

Re (between 5 and 50) performs the steady regime with the steady wake forming two symmetrically placed vortices on each side of the wake, for higher $Re > 50$ the flow becomes unsteady with an oscillatory wake containing a regular array of vortices moving downstream, known as the von Karman vortex street. With a further inctrease in Re, the flow becomes turbulent.

The reason why the flow over a cylinder is considered is because it is a model problem for a range of bluff body flow problems. A study of a flow past cylindrical bodies provides a general picture of the phenomenon of flow separation and bluff body wakes. By simulating the flow past the dimpled cylinder the effect of geometrical shape on the flow characteristics is studied. Since the problem is 2-dimensional the vorticity-streamfunction formulation of the Navier-Stokes system is used as an alternative of the primitive variables formulation. It reduces the total number of unknown functions from 3 (2 velocity components and pressure) to 2 (vorticity and streamfunction). In cartesian coordinates the system is the following

$$\frac{\partial \omega}{\partial t} - \frac{1}{Re}\Delta\omega = \frac{\partial \psi}{\partial x}\frac{\partial \omega}{\partial y} - \frac{\partial \psi}{\partial y}\frac{\partial \omega}{\partial x}$$

$$\omega = -\Delta\psi$$

Since it is difficult and in most cases even impossible to solve the Navier-Stokes system analytically, a variety of numerical methods has been developed to solve it numerically. One can divide numerical methods into two groups: local methods like finite difference methods (FDM), finite volume methods (FVM) and finite element methods (FEM), which are based on local approximation of derivatives of a function, and global methods such as spectral methods, where the approximations are global functions.

1.2 Spectral methods

Spectral methods represent a high order alternative to more standard methods like FDM and FEM. For smooth solutions, the discretization error of a spectral method for a decreases faster than any power of the resolution N (spectral convergence). Spectral methods use truncated series of smooth global functions for representation of the solution of a partial differential equation (PDE). In other words, the unknown function $u(x)$ is approximated by the truncated sum of global basis functions $\phi_k(x)$:

$$u(x) \approx u_n(x) = \sum_{k=0}^{n} a_k \phi_k(x)$$

Basis functions ψ_k in spectral methods are global orthogonal polynomials. The best choice for the basis functions depends on the type of the spatial domain, boundary conditions and the type of PDEs. Fourier polynomials are used as basis functions for problems periodic boundary conditions, and eigenfunctions of singular Sturm-Liouville problem are applied for non-periodic problems [18, 4]. For PDEs in bounded regions, Chebyshev and Legendre polynomial based spectral methods are used, while Laguerre (singular) and Hermite (non singular Sturm-Liouville problem) polynomials can be applied on unbounded regions [4, 16].

There are three types of spectral methods: spectral Galerkin, spectral Tau and spectral collocation (pseudospectral) methods. Consider the differential equation

$$Lu(x) = f(x) \quad x \in X$$

where L is the differential operator. Substituting the approximation u_N of the solu-

tion into the differential equation we define the residual:

$$R_N(x) = Lu_N(x) - f(x).$$

Residual minimization strategy and the type of test functions define the type of spectral methods. Galerkin and Tau methods are two weighted residual methods where for some set of test functions ψ_k the scalar product $(\psi_k, R_N(x)) = 0$, $k = 0, 1, ..., N$. In these methods coefficient of global expansion a_k are unknown. In the Galerkin method trial functions are some linear combinations of orthogonal polynomials that fulfill the boundary conditions. In the Tau method test functions ψ_k don't need to satisfy boundary conditions and are chosen to be the same as the spectral basis functions. Pseudospectral method (PSM) is based on the interpolation at a set of $N + 1$ collocation points $\{x_k\}_{k=0}^{N}$, in other words the residual function

$$F_N(x_k) = 0 \quad k = 0, 1, ..., N.$$

In PSM we take the grid point values of the approximate solution $u_N(x_k)$ as unknowns instead of the series coefficients a_k.

$$u_N(x_j) = \sum_{k=0}^{n} u_N(x_k)\phi_k(x_j) \quad j = 0, 1, ..., N.$$

The set of collocation points depends on the chosen basis set. The following condition must be satisfied $\psi_k(x_j) = \delta_k j$. PSM is the simplest among all spectral methods and allows the maximum flexibility while maintaining the good convergence properties of spectral approximations.

1.3 Solution on the infinite domain

In most cases, numerical methods are applied for bounded regions, where fluid flow around a solid body is considered within a finite area and boundary conditions are imposed on the external boundary. For exterior flows various boundary conditions are based on prediction of behavior of media far from the immersed body and sometimes have low order of accuracy. In order to get an accurate solution, the domain around the solid body has to be large enough to have a uniform flow on the outer boundary. High order method such as spectral methods are very sensitive to the accuracy of farfield boundary conditions.

Choosing a farfield boundary conditions, one can consider the whole infinite region around the body. One possibility is to map the infinite physical domain onto some bounded computational domain.

In this project, the pseudospectral method based on Fourier and Chebyshev expansions is used for spatial discretization of the Navier-Stokes system. Because of their global approximation spectral methods give highly accurate solutions on relatively small grids, but the basic version is restricted to simple geometries. To handle problems with complex geometries spectral elements [49] or other multidomain techniques [37, 38] are often used. These methods give geometrical flexibility, but appear to be difficult to implement. In cases when a complex domain can be mapped onto a simple rectangular and circular domain, a less expensive single domain spectral method can be implemented.

In this work, the physical domain is semi-infinite and has complex boundary (dimples). The transformation of the semi-infinite domain onto a unit disk is performed

and the Navier-Stokes system is rewritten in the new curvilinear coordinate system using metric tensor components. It gives flexibility in defining the transformations between coordinate systems. The importance of a properly defined transformation for the accuracy of results will be shown by numerical experiments.

1.4 Organization

This project is organized as follows. Chapter 2 gives a literature survey of spectral methods applied to fluid mechanics. Chapter 3 is devoted to the formulation of the problem on the unit disk. First, the problem, including governing system of equations in vorticity-streamfunction formulation and all boundary conditions, is defined. Then, the formulation of the problem on the unit disk is obtained in metric tensor form. At the end of the chapter 3, formulas for the computation of the drag and lift using numerical values for the vorticity are obtained.

Chapter 4 is devoted to the numerical method, it contains two parts. In the first part, we discuss the space discretization, in the second part solution techniques for the steady and unsteady problems are presented. The space discretization of the governing system on the unit disk is based on the Fourier-Chebyshev pseudospectral method. The computational grid on the unit disk is defined using Fornberg's strategy [14], which avoids a clustering of grid points near the origin and the coordinate singularity at the origin. Trefethen's implementation of Poisson solver on the unit disk in Matlab [47] is used as a base to construct matrices of pseudospectral approximation of the governing system. Then, solution of the resulting linear system of equations and the preconditioning with finite difference method is described.

Newton's method is implemented to solve the non-linear steady problem and semi-implicit Adams-Bashforth/Backward differentiation scheme is applied to the unsteady problem. The vorticity-streamfunction formulation leads to an overdetermined PDE for the streamfunction, while the vorticity equation has no boundary condition. To overcome this problem, both the streamfunction and vorticity equations are solved simultaneously.

In chapter 5, results of both steady and unsteady simulations are presented. For the numerical validation of the algorithm for the steady flow problem, spectral accuracy is demonstrated, and results of simulations of the steady flow past a smooth cylinder are compared with results previously obtained experimentally and numerically by other authors. Then, some steady simulation of the flow past dimpled cylinder are discussed. To test the unsteady code, simulations of flow past a smooth cylinder are also compared with results of other authors. After that, some results for the dimpled cylinder are obtained and discussed. In chapter 6, the main results and future work are discussed. We believe that we have the most accurate numerical results in the literature for flow over a smooth cylinder. We also have accurate numerical results for the dimpled cylinder case.

Chapter 2

Literature review

2.1 Spectral methods

Although spectral methods were founded and studied for a long time before computers, they became popular for applications to complex nonlinear problems in fluid mechanics and meteorology around the late 1970s. In 1977, modern spectral methods were reviewed by Gottlieb and Orszag in their monograph [18], where the theory on the Galerkin and Tau spectral methods was presented and application to fluid dynamical problems were discussed. Later, a further development of a theory of spectral methods, with focus on the pseudospectral method was presented in proceedings of a symposium on Spectral Methods for Partial Differential Equations edited by Voigt, Gottlieb and Orszag [51].

Since then, several other books have appeared. Among them Funaro's [16] which is devoted to spectral methods based on orthogonal polynomials. Boyd's book [4] gives an extensive description on the Fourier and Chebyshev spectral methods (600 pages long!) and their applications to eigenvalue, boundary value and time-dependent problems. In addition to Chebyshev and Fourier polynomials the book also discusses other possible basis functions for spectral approximations. Fornberg's in his book [14] showed, that pseudospectral methods can be viewed as special cases of FDM.

Pseudospectral methods employ collocation points which are specific for every

set of polynomial functions. Hence collocation grid can be defined for simple rectangular and circular domains. Pseudospectral methods can be applied on irregular domain using coorinate transformation. Since there are many cases where a smooth domain can be mapped onto the unit disk, the problem of solving PDEs on the unit disk was widely studied in the literature. In particular the solution of the Poisson equation is involved in many applications, for example the steamfunction equation in $\omega - \psi$ formulation of the Navier-Stokes system. Several solvers were developed for the Poisson problem on a unit disk. The Poisson equation on the unit disk is usually solved in polar coordinates using Chebyshev (or Legendre) expansions in radial direction and Fourier expansions in angular direction [5, 21, 22, 44]. The main problem in solving PDEs in polar, cylindrical and spherical geometries is a singularity at the pole. The numerical treatment of these singularities have been studied and a variety of approaches is available in literature [4, 22, 26, 46]. One way is to consider the pole as a boundary point and impose numerical boundary conditions at it. Huang and Sloan [22] used differential equations to impose pole conditions. Pole conditions applied to Navier-Stokes equations on a unit disk can be found in [26, 46]. Pole conditions are also discussed in Boyd [4].

Using pole conditions leads to some numerical difficulties such as the necessity of clustering grid point near the pole in radial direction. The maximum allowable time step in explicit and semi-explicite schemes is controlled by Courant-Friedrichs-Lewy (CFL) number [4]. It is observed that the clustering of nodes near the boundaries has an impact on the maximum CFL number. Hence, avoiding of clustering points near the pole gives an improvement on the CFL number [14]. A proper redefining of the numerical domain solves the problem with unwanted clustering. Different

strategies of redefining the domain were suggested by Fornberg [14] and by Heinrichs in [21], in both cases no polar conditions are needed because the point $r = 0$ is not in the computational domain. In [14] Fornberg suggested the strategies for both polar and spherical coordinates, where instead of taking Chebyshev expansions on the half interval $[0, 1]$ expansions on the full interval $[-1, 1]$ are applied with even number of collocaton points, and then using the symmetry condition:

$$u(r, \theta) = u(-r, (\theta + \pi) \mod 2\pi)$$

the actual computations are reduced to the half interval $[0, 1]$. The MATLAB implementation of the Poisson solver on the unit disk using Chebyshev expansions over the interval $[-1, 1]$ was presented by Trefethen in [47]. Heinrichs in [21] suggested the diameter approach where standard Chebyshev nodes defined on $[-1, 1]$ are used in radial direction and overlapping of collocation points is avoided by a special definition of nodes in angular direction. As in Fornberg's approach by using an even number of Chebyshev nodes an application of pole condition is avoided. In addition to that, another spectral collocation scheme for the Poisson problem on the unit disk was introduced in [21]. Heinrichs also suggested a direct mapping of the unit square onto the unit disk by means of an interpolation technique [21]. In this case the polar singularity problem is avoided. Heinrichs also shows how his approaches (diameter and unit square approach) work for more complex geometries. Torres and Coutsias in [46] also use the diameter approach in the spectral Tau method.

Matrices resulting from spectral approximation of differential equations have large condition number that grows with the number of nodes. In [17] Funaro and Heinrichs showed that the matrix of one-dimensional Chebyshev (or Legendre) spectral

approximation of the biharmonic operator has a very large condition number growing as $O(N^8)$, where N is the maximal degree of interpolating polynomials. Later Heinrichs proposed to apply a recombination of the basis of Chebyshev (Legendre) polynomials $\{p_N\}$ such that basis functions satisfy the homogenous boundary conditions. He applied polynomials of the form $(1-x^2)(1-y^2)p_{N-2}$ to elliptic equation and $(1-x^2)^2(1-y^2)^2p_{N-2}$ to a biharmonic equation in two-dimensional space, and showed that condition number for the second order problem is reduced to $O(N^2)$ and for the fourth order problem to $O(N^4)$ by the stabilizing technique [19].

Pseudospectral matrices are dense, due to global approximation, and have large condition number: it is $O(N^{2p})$ for Chebyshev and Legendre matrices of p-th order differential equations. Hence, the linear system of equations that arises from the pseudospectral approximation is usually solved using a preconditioned iterative technique. In 1980, Orszag suggested the usual second order second order finite difference approximation of the same differential operator as a preconditioner [35]. The main problem here is that an uneven distribution of collocation nodes is used in non-periodic case. The second order finite difference approximations of the first and second derivative of a function for unevenly distributed nodes can be found in [4]. Another option is to use an algorithm for finding weights of an approximation of any derivative of a function on any arbitrary set of unrepeated points is presented in [14]. This algorithm can be used to find finite difference coefficients of approximations of any order derivatives with different order of accuracy, depending on a number of nodes in a stencil. Finite difference preconditioning is also discussed in [20], where the FD operator is defined for boundary points using an outer point. Among other ways of preconditioning, the FEM can also be used [10].

2.2 Spectral methods in fluid mechanics

Spectral methods provide an advance approach to simulating fluid flow. Since 1970s application of spectral methods to various fluid flow problems was extensively studied by many researches. Among recent books on this subject one can find [12, 37]. In most applications, spectral methods are used for the special discretization of the Navier-Stokes equations, and finite difference methods are used for the time integration. Peyret in his book [37] describes an application of spectral methods to viscous fluid flow. He discusses solution techniques for the Navier-Stokes problems in the primitive variables pressure-velocity ($p - \mathbf{u}$) and in vorticity-streamfunction ($\omega - \psi$) using spectral approximation in spatial domain, and covers various time integration methods. Nowdays development of high-order methods which can be applied to flow problems with some complex geometry is one of the main interests of researches in this area [12, 21, 35, 41, 49]. The book written by Deville, Fischer and Mund [12] provides an advance survey on implementation of spectral methods to modeling fluid flows in irregular domains.

Solutions of various formulations of Navier-Stokes equations can be found in literature. However most three-dimensional problems are solved in the primitive ($p - \mathbf{u}$) variables. A Fourier–Chebyshev spectral collocation simulation of three-dimensional incompressible flow past an elliptic cylinder [33] was implemented by Mittal and Balachandar, and later a flow past spheroid was presented by Mittal in [34]. In both works, the semi-infinite domain around bluff body was truncated to the finite computational domain and special boundary conditions were posed on the inflow and outflow portions of the outer boundary. Solution of the $p - \mathbf{u}$

formulation of the Navier-Stokes equations in cylindrical geometries using spectral methods can be found in [30, 31, 39]. Lopez, Marques and Shen [30] implemented the spectral-Galerkin method for simulation of three-dimensional incompressible flows in a cylinder. Priymak and Miyazakiy [31, 39] used a pseudospectral method base on Fourier and Chebyshev expansions to study turbulent pipe flows.

In the two-dimensional case it is advantageous to use the $\omega - \psi$ formulation of the Navier-Stokes system, because two differential equations are solved comparing with three equations in $p - \mathbf{u}$ formulation. Solutions of the vorticity-streamfunctions formulation in polar coordinates using Fourier-Chebyshev expansions can be found in [46, 8]. In rectangular geometries either Chebyshev expansions [37] or Legendre expansions [2] are used in both directions. Parallel implementations of two-dimensional flow simulation by Fourier-Galerkin pseudospectral method were studied in [56]. Huang and Tang solved steady Navier-Stokes equations inside a circular boundary using Legendre collocation method in radial direction [23]. On the other hand, the $\omega - \psi$ formulation leads to an overdetermined Poisson equation for the stream-function and raises a question of finding a proper boundary condition for the vorticity. An influence matrix method is often used to impose boundary conditions [37].

In streamfunction formulation the non-linear fourth order (biharmonic) equation with two boundary conditions is solved. Schultz, Lee and Boyd [43] solved the driven cavity problem in the pure streamfunction formulation. Heinrichs [20] applied spectral multigrid method to the fourth-order equation for the streamfunction, splitting the equation into system of two stokes equations. Multidomain technique was applied to the pure streamfunction formulation of the Navier-Stokes equation

on the L-shape domain by Phillips and Malek in [38]. Karageorghis and Tang in [26] studied spectral domain decomposition method for solution of steady Navier-Stokes equation in circular geometries and noted, that reliable solutions in the streamfunction formulation can be obtained for a much smaller Reynolds number, than in the vorticity-streamfunction formulation.

Solution of Navier-Stokes equations in vorticity-velocity ($\omega - \mathbf{u}$) variables using spectral method was first presented by Clercx [7]. Spectral element method was implemented to $\omega - \mathbf{u}$ formulation for both two- and three-dimensional problem by Trujillo and Karniadakis [49], in particular, two- and three-dimensional flow past a cylinder were studied.

Since the Navier-Stokes equations are non-linear and time dependent various schemes for the time integration have been developed. These methods can be divided into 3 groups: explicit, semi-implicit and fully-implicit schemes. For different order time discretization methods used in spectral methods for fluid flow problems and stability analysis see Peyret's [37]. As a result of studying different schemes, $k - th$ order Adams-Bashforth/Backward-Differentiation (AB/BDIk) schemes are recommended for the semi-implicit time discretization and the fourth order Runge-Kutta/Crank-Nicolson as an explicit time integration. However classical AB/BDIk time discretization of the Navier-Stokes equations provide severe restrictions on the time step, when applied for high-Reynolds number flows. One can avoid that using the splitting method [55], where the full problem is split into an explicit transport step where for example Runge-Kutta scheme can be applied, and an implicit diffusion step, which can be discretized with an implicit $k-th$ order Backward-Differentiation.

In spectral methods the influence matrix method is commonly used to impose

apriori unknown boundary conditions for pressure in the $p-\mathbf{u}$ formulation or vorticity in the $\omega - \psi$ and $\omega - \mathbf{u}$ formulations computation in the solution of the Navier-Stokes system. The main idea of the influence matrix method is to consider the solution as a superposition of solutions of elementary problems with known boundary conditions. This technique can be successively applied to Stokes (linear) problems, which arise from the semi-implicit time-discretization of the Navier-Stokes system. Kleiser and Schumann introduced this technique for pressure-velocity equations [28, 51]. An application of the influence matrix method to the vorticity-streamfunction formulation was introduced in [50]. Applications to the vorticity-velocity formulation can be found in [7, 49]. Basic principles of the influence matrix method and different aspects of its application to both $\omega - \psi$ and $p - \mathbf{u}$ formulations can be found in [37]. A technique very similar to the influence matrix method was applied by Chou for a steady vorticity-streamfunction formulation of the Navier-Stokes system in [6]. One of the main disadvantages of the influence matrix method is that it requires a lot of memory and it becomes especially difficult in three-dimensional unsteady flow applications. For some solutions of storage problem see [37].

2.3 Fluid flow past bluff bodies

The flow past bodies immersed in a fluid has been studied for a long time because of its importance in aero- and hydrodynamic applications. A flow over a cylinder is considered as a model problem for a range of bluff body flow problems. A study of a flow past cylindrical bodies provides a general picture of the phenomenon of flow separation and bluff body wakes. Flow behind a circular cylinder has been extensively

studied experimentally and numerically by many authors (see Williamson's review [54]). The flow over a cylinder is also is used as a benchmark to test new numerical methods [36, 40]. There are works devoted to numerical simulations of symmetric (steady) flow over the circular cylinder, see, for example, Fornberg [13] and Dennis and Chang [11]. Among others, simulations of unsteady flows past circular cylinder were presented in [27, 36]. The Fourier-Chebyshev spectral collocation simulation of three-dimensional incompressible flow past an elliptic cylinder were implemented by Mittal and Balachandar [33].

Chapter 3

System of equations and boundary conditions

3.1 Formulation of the problem on the physical domain

The flow of an incompressible viscous fluid is described by the Navier-Stokes equations. In cartesian coordinates the two-dimensional pressure-velocity formulation of the system is

$$\frac{\partial u}{\partial t} + u\frac{\partial u}{\partial x} + v\frac{\partial u}{\partial y} - \frac{1}{Re}\Delta u = -\frac{\partial p}{\partial x}, \tag{3.1}$$

$$\frac{\partial v}{\partial t} + u\frac{\partial v}{\partial x} + v\frac{\partial v}{\partial y} - \frac{1}{Re}\Delta v = -\frac{\partial p}{\partial y}, \tag{3.2}$$

$$\frac{\partial u}{\partial x} + \frac{\partial v}{\partial y} = 0, \tag{3.3}$$

here $\mathbf{u} = (u, v)$ is the velocity vector and p is the pressure. The Reynolds number for the circular cylinder with diameter d, based on the radius $a = d/2$ is

$$Re = \frac{\rho U a}{\mu}, \tag{3.4}$$

here ρ and μ are density and dynamic viscosity of a fluid, and U is a uniform velocity of a flow at infinity.

The pressure in $(p-\mathbf{u})$ formulation is computed from the incompressibility condition (3.3) using velocity boundary conditions. The pressure in this case is defined up to a constant and the constant is evaluated by the additional constraint $\int_S p ds = 0$ (S is the entire region of the problem). For the two-dimensional problem, the vorticity-streamfunction formulation of the Navier-Stokes system, where the streamfunction

ψ and vorticity ω are defined by

$$u = \frac{\partial \psi}{\partial y}, \qquad v = -\frac{\partial \psi}{\partial x}, \qquad \omega = \frac{\partial v}{\partial x} - \frac{\partial u}{\partial y}, \tag{3.5}$$

replaces the two momentum equations by one equation. It also eliminates the pressure from calculations and the incompressibility condition (3.3) is satisfied automatically by the construction:

$$\frac{\partial u}{\partial x} + \frac{\partial v}{\partial y} = \frac{\partial^2 \psi}{\partial x \partial y} - \frac{\partial^2 \psi}{\partial x \partial y} = 0.$$

The vorticity momentum equation is obtained from (3.1), by taking $\partial/\partial y$ of the first equation and $-\partial/\partial x$ of the second equation and adding them together. Then, using definitions of the vorticity and streamfunction (3.5), it can be shown that:

$$\frac{\partial \omega}{\partial t} - \frac{2}{Re}\Delta\omega = G(\omega, \psi), \tag{3.6}$$

where

$$G(\omega, \psi) = \frac{\partial \psi}{\partial x}\frac{\partial \omega}{\partial y} - \frac{\partial \psi}{\partial y}\frac{\partial \omega}{\partial x} = \begin{vmatrix} \frac{\partial \psi}{\partial x} & \frac{\partial \psi}{\partial y} \\ \frac{\partial \omega}{\partial x} & \frac{\partial \omega}{\partial y} \end{vmatrix}. \tag{3.7}$$

For the streamfunction the Poisson equation is obtained

$$\omega = \frac{\partial v}{\partial x} - \frac{\partial u}{\partial y} = -\frac{\partial^2 \psi}{\partial x^2} - \frac{\partial^2 \psi}{\partial y^2} = -\Delta\psi. \tag{3.8}$$

To state the problem we need to define the domain, where the system (3.6-3.8) is satisfied. For simplicity the dimpled surface is represented by the cosine function parameterized by the polar angle θ:

$$\gamma(\theta) = 1 + \epsilon \cos(c\theta), \qquad 0 \le \theta < 2\pi, \tag{3.9}$$

here c is the number of dimples and ϵ is their size (depth).

In most cases the flow past cylinder is considered within a truncated bounded region with farfield boundary condition [33]. Also for accurate results the distance between the cylinder and the outer boundary has to be large enough. When a global spatial discretization is applied, the influence of the lateral boundary is even more important and choosing appropriate outer boundary conditions (inflow and outflow) is a challenge. As an alternative we consider a semi-infinite domain instead and impose the boundary condition at infinity.

Let Ω be a semi-infinite domain with the boundary Γ, defined by

$$\Gamma = (\Gamma_x, \Gamma_y) = (\gamma(\theta)\cos(\theta), \gamma(\theta)\sin(\theta)). \tag{3.10}$$

On the solid boundary no-slip conditions are imposed. In the $\omega - \psi$ formulation there are two boundary conditions for the streamfunction:

$$\psi = \frac{\partial \psi}{\partial \vec{n}} = 0 \quad on \quad \Gamma, \tag{3.11}$$

where $\vec{n}$ is an outer normal vector to the boundary (3.10), and no boundary conditions for the vorticity. The flow at the infinity is uniform so that the velocity vector is $\mathbf{u}_\infty = (\psi_y, -\psi_x) = (1, 0)$. Hence for the streamfunction we get the following condition

$$\psi \to y + C, \quad \omega \to 0 \quad as \quad r = \sqrt{x^2 + y^2} \to \infty. \tag{3.12}$$

To determine the constant C, consider the streamline that ends up at the stagnation point (the heavy line on fig.3.1). The value ψ is constant along this line and from the boundary condition (3.11) $\psi = 0$ at stagnation point. Then at the infinity along the zero streamline we get $\psi = C = 0$.

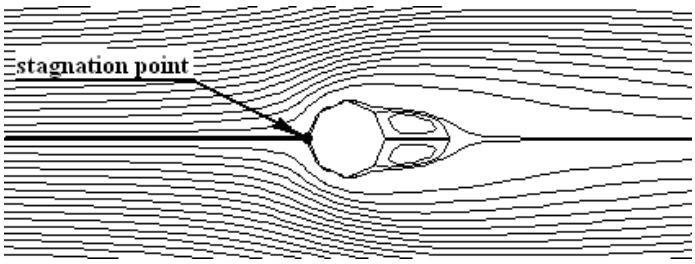

Figure 3.1: Streamline to the stagnation point

3.2 Formulation on the unit disk

The problem (3.6,3.8,3.11) is defined on the semi-infinite domain Ω with irregular boundary Γ. Collocation grid in pseudospectral method can be defined only on simple geometries such as unit disk. Hence, the problem (3.6,3.8,3.11) has to be rewritten for the unit disk.

In this section the transformation between the unit disk $E = \{(R, \theta),\ 0 \leq R \leq 1,\ 0 \leq \theta \leq 2\pi\}$ and the semi-infinite domain Ω is defined. The transformation is such that the center of the unit disk (the origin) corresponds to the infinity in Ω and the boundary of the unit disk corresponds to the boundary Γ.

Let $(x, y) \in \Omega$ be the point in the physical domain and $(R, \theta) \in E$ be the point in the computational domain. The transformation from the computational domain to the physical domain $W : E \to \Omega$ is defined by

$$W(R, \theta) = (x, y) = [f(R)\gamma(\theta)]\,(\cos\theta, \sin\theta). \tag{3.13}$$

The transformation (3.13) states that if we define the position of the point using polar coordinates, then the point along the line with fixed angle θ is mapped by changing the radius: $R \to f(R)\gamma(\theta)$. Here $\gamma(\theta)$ produces dimples and $f(R)$ maps $R \in [0, 1]$

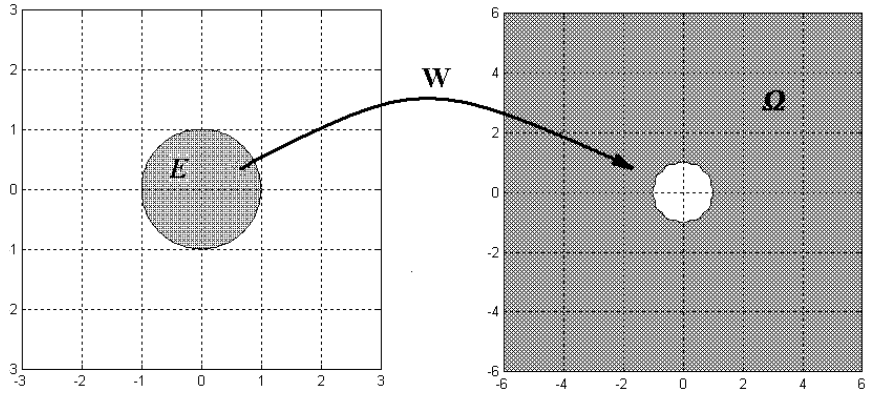

Figure 3.2: The map from the unit disk to the semi–infinite domain around dimpled cylinder

to $f(R) \in [1; \infty)$. Hence the map $f(R)$ must satisfy the following constrains:

$$\begin{aligned} &f(1) = 1, \\ &\lim_{R\to 0} f(R) = \infty, \\ &\tfrac{\partial f}{\partial R} < 0. \end{aligned} \tag{3.14}$$

The exact functional $f(R)$ is discussed in section 4.1.3.

Now we write the Jacobian of the transformation (3.13):

$$J = \begin{bmatrix} \partial_R x & \partial_\theta x \\ \partial_R y & \partial_\theta y \end{bmatrix} = \begin{bmatrix} f'(R)\gamma(\theta)\cos\theta & f(R)\gamma'(\theta)\cos\theta - f(R)\gamma(\theta)\sin\theta \\ f'(R)\gamma(\theta)\sin\theta & f(R)\gamma'(\theta)\sin\theta + f(R)\gamma(\theta)\cos\theta \end{bmatrix}, \tag{3.15}$$

here $\partial_R = \frac{\partial}{\partial R}$, $\partial_\theta = \frac{\partial}{\partial \theta}$.

Then the induced covariant metric tensor of the embedding (3.13) is

$$g = J^T J = \begin{bmatrix} f'(R)^2\gamma(\theta)^2 & f(R)f'(R)\gamma(\theta)\gamma'(\theta) \\ f(R)f'(R)\gamma(\theta)\gamma'(\theta) & f(R)^2(\gamma(\theta)^2 + \gamma'(\theta)^2) \end{bmatrix} = \begin{bmatrix} g_{RR} & g_{R\theta} \\ g_{\theta R} & g_{\theta\theta} \end{bmatrix}. \tag{3.16}$$

Note that the metric tensor g is symmetric and positively definite and its determinant

is

$$|g| = g_{RR}g_{\theta\theta} - g_{R\theta}^2 = \gamma(\theta)^4 f'(R)^2 = |J|^2. \tag{3.17}$$

The Laplacian in the tensor form is

$$\Delta = \frac{1}{\sqrt{|g|}}\partial_j \left[\sqrt{|g|}g^{ij}\partial_i\right], \quad i,j = R,\theta, \tag{3.18}$$

here g^{ij} are components of the inverse of the covariant metric tensor, which is also called the contravariant metric tensor. Since we are dealing with a two-dimensional space, the components of the contravariant metric tensor can be derived from

$$\begin{aligned} g^{RR} &= \tfrac{g_{\theta\theta}}{|g|} = \tfrac{\gamma(\theta)^2+\gamma'(\theta)^2}{\gamma(\theta)^4 f'(R)^2}, \\ g^{R\theta} = g^{\theta R} &= -\tfrac{g_{R\theta}}{|g|} = -\tfrac{\gamma'(\theta)}{\gamma(\theta)^3 f(R) f'(R)}, \\ g^{\theta\theta} &= \tfrac{g_{RR}}{|g|} = \tfrac{1}{\gamma(\theta)^2 f(R)^2}. \end{aligned} \tag{3.19}$$

Components of the covariant, contravariant metric tensor and the Laplacian for a given embedding can be computed in Maple (see `http://www.aere.iastate.edu/ave/viscous_flow/files/maple.html`).

Using (3.17-3.19) we derive

$$\partial_R(\sqrt{|g|}g^{RR}) = \frac{(\gamma(\theta)^2+\gamma'(\theta)^2)(f'(R)^2 - f(R)f''(R))}{\gamma(\theta)^2 f'(R)^2},$$

$$\partial_\theta(\sqrt{|g|}g^{R\theta}) = \frac{\gamma'(\theta)^2 - \gamma(\theta)\gamma''(\theta)}{\gamma(\theta)^2},$$

$$\partial_R(\sqrt{|g|}g^{R\theta}) = 0, \quad \partial_\theta(\sqrt{|g|}g^{\theta\theta}) = 0.$$

Then plugging to (3.18) we reduce the number of elements in the Laplacian:

$$\Delta = g^{RR}\frac{\partial^2}{\partial R^2} + 2g^{R\theta}\frac{\partial^2}{\partial R\theta} + g^{\theta\theta}\frac{\partial^2}{\partial\theta^2} + g^R\frac{\partial}{\partial R}, \tag{3.20}$$

where

$$g^R = \frac{1}{\sqrt{|g|}}\left[\partial_R(\sqrt{|g|}g^{RR}) + \partial_\theta(\sqrt{|g|}g^{R\theta})\right]. \tag{3.21}$$

The condition at infinity (3.12) provides that

$$\psi \to f(R)\gamma(\theta)sin(\theta) \quad as \quad R \to 0.$$

Since $\lim_{R\to 0} f(R) = \infty$, the resulting solution for the streamfunction will blow up at the origin of the unit disk E. As an alternative we define the function

$$\phi = \psi - y. \tag{3.22}$$

From the above definition, the condition (3.12) becomes

$$\phi \to 0, \quad \omega \to 0 \quad as \quad \sqrt{x^2+y^2} \to \infty, \quad or \quad R \to 0. \tag{3.23}$$

Since $\Delta y = 0$, the Poisson equation for the new function isn't changed and the Navier-Stokes system is reformulated as follows

$$\frac{\partial \omega}{\partial t} - \frac{1}{Re}\Delta\omega = G(\omega, \phi), \tag{3.24}$$

$$\omega = -\Delta\phi, \tag{3.25}$$

where

$$G(\omega,\phi) = \frac{\partial(\phi+y)}{\partial x}\frac{\partial \omega}{\partial y} - \frac{\partial(\phi+y)}{\partial y}\frac{\partial \omega}{\partial x} = \begin{vmatrix} \frac{\partial(\phi+y)}{\partial x} & \frac{\partial(\phi+y)}{\partial y} \\ \frac{\partial \omega}{\partial x} & \frac{\partial \omega}{\partial y} \end{vmatrix}. \tag{3.26}$$

No-slip boundary conditions (3.11) become

$$\begin{aligned} \phi &= -y \quad on \quad \Gamma, \\ \tfrac{\partial \phi}{\partial \vec{n}} &= -\tfrac{\partial y}{\partial \vec{n}} \quad on \quad \Gamma. \end{aligned} \tag{3.27}$$

Now the convective term (3.26) in new coordinate system is obtained. First we note that

$$\begin{bmatrix} \partial_R\psi & \partial_\theta\psi \\ \partial_R\omega & \partial_\theta\omega \end{bmatrix} = J \begin{bmatrix} \partial_x\psi & \partial_y\psi \\ \partial_x\omega & \partial_y\omega \end{bmatrix}.$$

Then by taking the determinant of both sides we get

$$G(\omega,\phi) = \frac{1}{|J|}\begin{vmatrix} \partial_R(\phi+y) & \partial_\theta(\phi+y) \\ \partial_R\omega & \partial_\theta\omega \end{vmatrix} = \frac{1}{|J|}\begin{vmatrix} \partial_R\phi + J_{21} & \partial_\theta\phi + J_{22} \\ \partial_R\omega & \partial_\theta\omega \end{vmatrix}$$

or

$$G(\omega,\phi) = \frac{1}{|J|}\left(\frac{\partial\phi}{\partial R}\frac{\partial\omega}{\partial\theta} - \frac{\partial\phi}{\partial\theta}\frac{\partial\omega}{\partial R}\right) + \frac{J_{21}}{|J|}\frac{\partial\omega}{\partial\theta} - \frac{J_{22}}{|J|}\frac{\partial\omega}{\partial R}. \tag{3.28}$$

In present computations, it is necessary to know the expressions for the normal and tangential derivatives on the boundary. These formulas are obtained using metric tensor components:

$$\frac{\partial}{\partial\vec{n}}|_\Gamma = \frac{1}{\sqrt{g^{RR}}}\left(g^{RR}\frac{\partial}{\partial R} + g^{R\theta}\frac{\partial}{\partial\theta}\right)|_{R=1}, \tag{3.29}$$

$$\frac{\partial}{\partial\vec{\tau}}|_\Gamma = \frac{1}{\sqrt{g_{\theta\theta}}}\frac{\partial}{\partial\theta}|_{R=1}. \tag{3.30}$$

From the Dirichlet condition for the streamfunction we can say that $\partial\psi/\partial\vec{\tau} = 0$ on the boundary as well, here $\vec{\tau}$ is a tangential vector to the boundary (3.10). Since both R and θ derivatives are linear combinations of normal and tangential derivatives, we may conclude that derivatives $\partial\psi/\partial R = \partial\psi/\partial\theta = 0$ on the boundary. Hence to simplify the second no-slip boundary condition one can take

$$\frac{\partial\psi}{\partial R}|_{R=1} = 0.$$

From (3.27) using (3.13) we obtain boundary conditions in the new coordinate sys-

tem.

$$\phi|_{R=1} = -\gamma(\theta)\sin(\theta) = q(\theta), \tag{3.31}$$

$$\frac{\partial \phi}{\partial R}|_{R=1} = -f'(1)\gamma(\theta)\sin(\theta) = h(\theta). \tag{3.32}$$

3.3 Computations of drag and lift coefficients

A solid body immersed in the fluid experiences a net force $\vec{F}$ due to the action of the fluid. For a viscous flow there are two components to the net force acting on a solid surface: forces due to pressure and to skin-friction. The first one is a contribution due to the fluid pressure differences over the surface of the body, it acts normally to the solid body surface. The second is due to shear stress and acts parallel to the surface of the body. The net force on the surface of the cylinder Γ resulting from shear stress σ_w and pressure p is

$$\vec{F} = \vec{F}_{pressure} + \vec{F}_{skin-friction}, \tag{3.33}$$

where

$$\vec{F}_{pressure} = -\int_{\Gamma} p\vec{n}ds \tag{3.34}$$

and

$$\vec{F}_{skin-friction} = \int_{\Gamma} \sigma_w \vec{\tau} ds. \tag{3.35}$$

Tangential $\vec{\tau}$ and normal $\vec{n}$ vectors can be obtained from the definition of the boundary (3.10). Shear stress σ_w on the solid wall in two-dimensional case can be defined by

$$\sigma_w = \mu \frac{\partial u_\tau}{\partial n} = -\mu\omega. \tag{3.36}$$

Note the last equality in (3.36) is due to the definition of the vorticity $\omega = \nabla \times \mathbf{u} = \frac{\partial u_n}{\partial \tau} - \frac{\partial u_\tau}{\partial n}$ and the fact that $\frac{\partial u_n}{\partial \tau} = 0$ on the solid wall.

Now using (3.36) we express the skin-friction force via vorticity

$$\vec{F}_{skin-friction} = -\mu \int_\Gamma \omega \vec{\tau} ds. \tag{3.37}$$

The component of the net force (3.33) parallel to the direction of motion is called the drag force F_D, and the force component perpendicular to the direction of the motion is the lift force, F_L. Directions of lift and drag forces for the dimpled cylinder are shown on fig.3.3. In computations the dimensionless lift and drag coefficients are

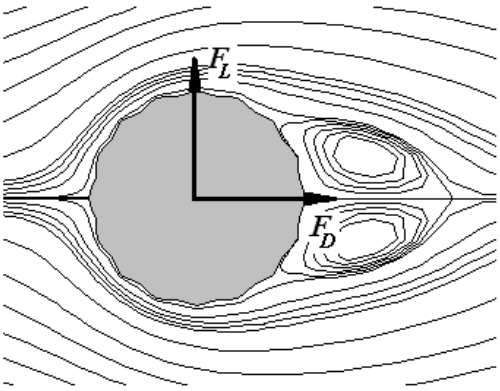

Figure 3.3: Drag and lift forces acting on the golf ball

evaluated instead of the forces themselves. The relations between dimensional drag F_D and lift F_L forces and their dimensionless coefficients are

$$C_D = \frac{2F_D}{\rho U^2 d}, \quad C_L = \frac{2F_L}{\rho U^2 d}.$$

Taking the x and y components of the net force we get the following formulas for

the drag and lift coefficients

$$C_D = -\int_\Gamma p n_x ds - \frac{1}{Re}\int_\Gamma \omega \tau_x ds, \tag{3.38}$$

$$C_L = -\int_\Gamma p n_y ds - \frac{1}{Re}\int_\Gamma \omega \tau_y ds. \tag{3.39}$$

Note that the vorticity ω and pressure p in (3.38) are dimensionless quantities meaning quantities without any physical units, while in (3.34-3.37) they are dimensional.

Now we rewrite formulas (3.38) to evaluate drag and lift coefficients using data obtained from the numerical solution of the problem (3.24-3.27). Let $\Gamma_i' = \frac{d\Gamma_i}{d\theta}$, $i = x, y$, then the unit tangent vector on the boundary Γ is

$$\vec{\tau} = (\tau_x, \tau_y) = \frac{1}{\sqrt{\Gamma_x'^2 + \Gamma_y'^2}}(\Gamma_x', \Gamma_y') \tag{3.40}$$

and the unit outward normal vector is

$$\vec{n} = (n_x, n_y) = (\tau_y, -\tau_x) = \frac{1}{\sqrt{\Gamma_x'^2 + \Gamma_y'^2}}(\Gamma_y', -\Gamma_x'). \tag{3.41}$$

Now using (3.40-3.41) and applying the formula for line integral on a curve with $ds = \sqrt{\Gamma_x'^2 + \Gamma_y'^2}d\theta$ to the (3.38), we get

$$C_D = \underbrace{-\int_0^{2\pi} p\Gamma_y'(\theta)d\theta}_{C_{D_p}} \underbrace{-\frac{1}{Re}\int_0^{2\pi} \omega\Gamma_x' d\theta}_{C_{D_f}}, \tag{3.42}$$

$$C_L = \underbrace{\int_0^{2\pi} p\Gamma_x'(\theta)d\theta}_{C_{L_p}} \underbrace{-\frac{1}{Re}\int_0^{2\pi} \omega\Gamma_y' d\theta}_{C_{L_f}}. \tag{3.43}$$

To evaluate the pressure terms C_{D_p} and C_{L_p} using numerical data for the vorticity, obtained by solving the problem, the relation between the pressure and the vorticity is needed. Therefore consider the momentum equation of the Navier-Stokes system:

$$\frac{\partial \mathbf{u}}{\partial t} + \nabla \mathbf{u} \cdot \mathbf{u} - \frac{1}{Re}\Delta \mathbf{u} = -\nabla p.$$

Using the vector identity $\nabla \times (\nabla \times \mathbf{u}) = \nabla(\nabla \cdot \mathbf{u}) - \Delta \mathbf{u}$, continuity equation $\nabla \cdot \mathbf{u} = 0$ and vorticity definition one can get that $\Delta \mathbf{u} = -\nabla \times \omega$. Now since $\mathbf{u} = 0$ on the solid boundary, then from the momentum equation we get the following relation between pressure and vorticity on the boundary:

$$\nabla p = -\frac{1}{Re} \nabla \times \omega.$$

Taking the dot product on both sides with $\vec{\tau}$

$$\vec{\tau} \cdot \nabla p = -\frac{1}{Re} \vec{\tau} \cdot \nabla \times \omega$$

we get, that on the boundary

$$\frac{\partial p}{\partial \vec{\tau}}|_{\Gamma} = \frac{1}{Re} \frac{\partial \omega}{\partial \vec{n}}|_{\Gamma}. \tag{3.44}$$

From (3.19) we get that

$$g_{\theta\theta} = |g| g^{RR}.$$

Then plugging the above expression to (3.29) and using the result in the relation (3.44), we obtain

$$\frac{\partial p}{\partial \theta}|_{R=1} = \frac{\sqrt{|g|}}{Re} \left(g^{RR} \frac{\partial \omega}{\partial R} + g^{R\theta} \frac{\partial \omega}{\partial \theta} \right) |_{R=1}. \tag{3.45}$$

The last result can be applied in the evaluation of the pressure components of the drag and lift coefficients using the integration by parts:

$$\int_0^{2\pi} p \Gamma_i' d\theta = p\Gamma_i|_0^{2\pi} - \int_0^{2\pi} \frac{\partial p}{\partial \theta} \Gamma_i d\theta = -\int_0^{2\pi} \frac{\partial p}{\partial \theta} \Gamma_i d\theta, \qquad i = x, y.$$

Now we obtain final formulas for the drag and lift coefficients by employing formulas

from integration by parts and using (3.45):

$$C_D = -\underbrace{\frac{1}{Re}\int_0^{2\pi}\left(\sqrt{|g|}g^{RR}\frac{\partial\omega}{\partial R}+\sqrt{|g|}g^{R\theta}\frac{\partial\omega}{\partial\theta}\right)|_{R=1}\Gamma_y d\theta}_{C_{D_p}} - \underbrace{\frac{1}{Re}\int_0^{2\pi}\omega\Gamma'_x(\theta)d\theta}_{C_{D_f}} \tag{3.46}$$

$$C_L = \underbrace{\frac{1}{Re}\int_0^{2\pi}\left(\sqrt{|g|}g^{RR}\frac{\partial\omega}{\partial R}+\sqrt{|g|}g^{R\theta}\frac{\partial\omega}{\partial\theta}\right)|_{R=1}\Gamma_x d\theta}_{C_{L_p}} - \underbrace{\frac{1}{Re}\int_0^{2\pi}\omega\Gamma'_y(\theta)d\theta}_{C_{L_f}} \tag{3.47}$$

For a flow over a circular cylinder or a sphere the drag coefficient, which is a function of Re number, behaves similarly. For $Re \leq 1$ there is no flow separation on the downstream side of the body and the drag is high and is predominantly friction drag. As Reynolds number increases, the drag coefficient decreases, at the same time the pressure force becomes larger and viscous effects become smaller (except near boundary). Flow begins to separate, the point of separation on the body surface is a point at which $\frac{\partial u_\tau}{\partial \vec{n}} = 0$, and hence the shear stress $\sigma_w = 0$. First two stationary eddies appear behind the sphere (or cylinder) and as Re increases, the eddies become unstable and start to break away in periodic fashion. For periodic flow the pressure force dominates the shear force.

The shape of the body determines the relative magnitudes of the two force components. Thus adding dimples to a surface of the solid body will change the drag and lift. For unsteady flows with large $Re \sim 10^5 - 10^6$ dimples reduce the drag by lowering the critical Re at which flow becomes turbulent ([1, 3, 15, 32]), this result is applied for instance in the golf ball production.

Chapter 4

Numerical method

4.1 Space discretization

4.1.1 Spectral collocation method

Among all spectral methods pseudospectral method became the most popular. It is the easiest and most flexible in terms of implementation and yet provides spectral convergence for smooth solutions. Pseudospectral methods are based on choosing the set of collocation points and making the residual function to be zero at these points. Consider an interpolating polynomial to the unknown function $u(x)$ for the set of $n+1$ collocation points $\{x_j\}_{j=0}^{n}$

$$P_n u(x) = \sum_{j=0}^{n} u(x_j) q_j(x), \tag{4.1}$$

where $q_j(x)$ are polynomials, satisfying $q_j(x_i) = \delta_{ji}$. Differentiating (4.1) s times at collocation point x_k we get a pseudospectral approximation of s-order derivation of the function $u(x)$ at this point:

$$\frac{d^s P_n u(x_k)}{dx^s} = \sum_{j=0}^{n-1} u(x_j) \left[\frac{d^s}{dx^s} q_j(x) \right]_{x_k} = \sum_{j=0}^{n-1} u(x_j) D_{kj}^{(s)},$$

here $D_{kj}^{(s)}$ are entries of a pseudospectral differentiation matrix of the s-order derivative $D^{(s)}$.

Now we apply pseudospectral method to our problem. Since it is formulated on a unit disk, the Chebyshev collocation method is used in radial direction while

the Fourier collocation method is used in angular direction. Consider a unit disk $E = \{(R, \theta), 0 \leq R \leq 1, 0 \leq \theta < 2\pi\}$. The discrete domain E_{nM} is defined, using Fornberg's pseudospectral approach for polar geometries [14]. In radial direction consider $N+1$ Chebyshev Gauss-Lobatto nodes defined on the entire interval $[-1, 1]$ instead of the half-interval $[0, 1]$:

$$R_j = \cos\left(\frac{\pi j}{N}\right), j = 0, 1, ..., N, \tag{4.2}$$

here $N = 2n + 1$ is an odd number. In this case nodes are clustered only near the boundary $R = 1$ and unnecessary clustering of nodes near the origin $R = 0$ is avoided. There are several advantages of such node distribution (see [14]): CFL condition is improved by avoiding clustering near the origin, so a larger time step can be used in computations, also by taking an even number $(N + 1)$ of Chebyshev nodes the polar singularity problem is avoided, because the origin is excluded from the discrete domain E_{nM}, so that no additional polar conditions are needed. In the angular direction consider $M = 2m$ Fourier collocation nodes:

$$\theta_k = \frac{2\pi k}{M}, \qquad k = 0, 1, ..., M - 1. \tag{4.3}$$

Chebyshev pseudospectral differentiation matrix for an even number of nodes defined by (4.2) can be found for example in [51] and is the following:

$$D_{kj} = \begin{cases} \frac{(-1)^{k+j}}{R_k - R_j}\frac{a_k}{a_j}, & k \neq j \\ -\frac{R_k}{2(1-R_k^2)}, & 1 \leqslant k = j \leqslant N-1 \\ \frac{2N^2+1}{6}, & k = j = 0 \\ -\frac{2N^2+1}{6}, & k = j = N \end{cases}, \quad where \;\; a_j = \begin{cases} 2, & j = 0, N \\ 1, & 1 \leq j < N \end{cases} \tag{4.4}$$

From (4.4) one may see that the Chebyshev pseudospectral derivative matrix is neither symmetric nor antisymmetric, that causes difficulties in computing the solution of the algebraic linear system, resulting from Chebyshev pseudospectral approximation. For the second order derivative $D^{(2)} = (D)^2$ can be used.

The Fourier pseudospectral matrix for an even number of collocation nodes is:

$$DF_{kj} = \begin{cases} 0, & k = j \\ \frac{(-1)^{k-j}}{2} \cot((k-j)\frac{h}{2}), & k \neq j \end{cases}$$

The resulting matrix DF is antisymmetric. Entries of the Fourier pseudospectral differentiation matrix of the second order for the same set of collocation nodes $DF^{(2)}_{kj}$ are

$$DF^{(2)}_{kj} = \begin{cases} -\frac{\pi^2}{3h^2} - \frac{1}{6}, & k = j \\ \frac{(-1)^{(k+1-j)}}{2\sin^2\left(\frac{(k-j)h}{2}\right)}, & k \neq j \end{cases}$$

Note that $DF^{(2)}$ is a symmetric matrix.

Now we have all pseudospectral differentiation matrices to define approximations for all differential operators of the problem (3.24-3.31).

4.1.2 Pseudospectral approximation of differential operators

To obtain pseudospectral approximation matrices for all differential operators $\frac{\partial}{\partial R}, \frac{\partial}{\partial \theta}$ and $L = -\Delta$ we use Trefethen's approach [47], implemented for the Laplacian operator on the unit disk using tensor product operation for matrices (Kronecker product).

The mesh defined by (4.2-4.3) is such that the map from (R, θ) to (x, y) is 2-to-1 (see fig. 4.1). Using the symmetry condition

$$u(R, \theta) = u(-R, (\theta + \pi) \mod 2\pi) \tag{4.5}$$

half of the domain $[-1,1]\times[0,2\pi]$ can be ignored, two options are shown on fig.4.2.

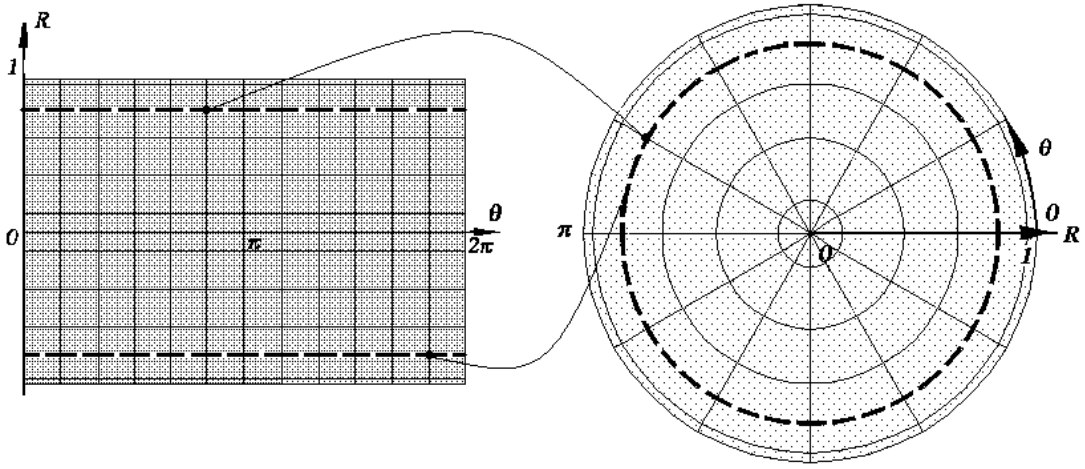

Figure 4.1: The map from $[-1,1]\times[0,2\pi]$ to a unit circle: two coordinate lines from cartesian grid are mapped to the same line on the unit circle.

Now we show how it works. Consider the expansion of the k-th derivative of an arbitrary function u in the radial direction using $N+1$ collocation points, where $N=2n+1$:

$$u^{(s)}(R_k,\theta)=\sum_{i=0}^{N}D^{(s)}_{ki}u(R_i,\theta)=$$

$$=\sum_{i=0}^{n}D^{(s)}_{ki}u(R_i,\theta)+\sum_{i=n+1}^{N}D^{(s)}_{ki}u(-R_{N-i},\theta)=$$

$$=\sum_{i=0}^{n}D^{(s)}_{ki}u(R_i,\theta)+\sum_{i=0}^{n}D^{(s)}_{k,N-i}u(-R_i,\theta)=$$

$$=\sum_{i=0}^{n}\left(D^{(s)}_{ki}u(R_i,\theta)+D^{(s)}_{k,N-i}u(R_i,(\theta+\pi)\mod 2\pi)\right).$$

Here we applied the definition of Chebyshev grid points (4.2) to get $R_{N-i}=-R_i$ and the symmetry condition (4.5). From the above result it is clear that only half of Chebyshev collocation nodes is needed.

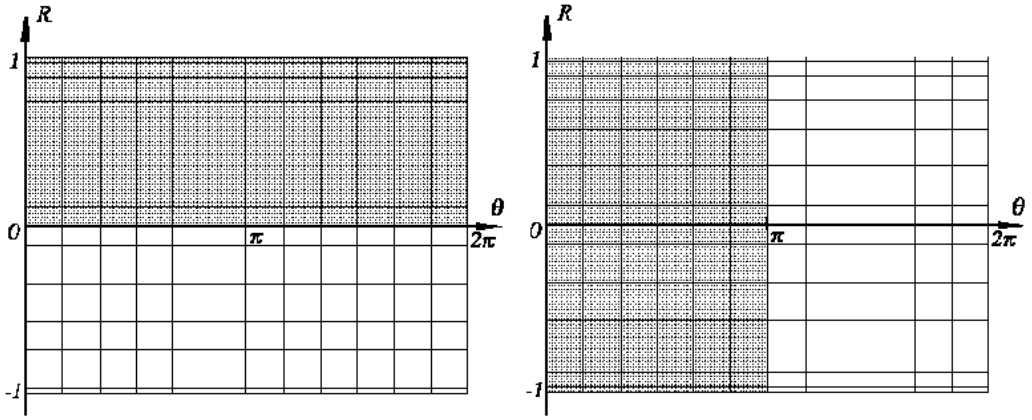

Figure 4.2: Possible choices for computational domain

Following Trefethen, the region for $R < 0$ is discarded in the present work. The collocation grid containing $dim = (n+1)M$ points is defined by

$$E_{nM} = \{(R_j, \theta_k), \quad j = 0, 1, ..., n, \quad k = 0, 1, ..., M-1\}, \tag{4.6}$$

here R_j and θ_k are defined by (4.3) and (4.2) respectively, describes the discrete domain, for an example of E_{nM} see fig.4.3. Now for an arbitrary matrix $A = \begin{bmatrix} a_0 & a_1 & ... & a_n \end{bmatrix}$ with columns $a_0, a_1, ..., a_n$, define the operation of flipping a matrix from left to right:

$$\tilde{A} = \begin{bmatrix} a_n & a_{n-1} & ... & a_0 \end{bmatrix}.$$

Consider the Chebyshev pseudospectral matrix D defined in (4.4) and let $D = \begin{bmatrix} \bar{D}_{11} & \bar{D}_{12} \\ \bar{D}_{21} & \bar{D}_{22} \end{bmatrix}$, where $\bar{D}_{ij}$ are $(n+1) \times (n+1)$ submatrices. Since the domain E_{nM} is defined for $R > 0$, we can discard parts $\bar{D}_{21}$ and $\bar{D}_{22}$ of the matrix D, but we still need to include an effect of the discarded regions, and hence the submatrix $\bar{D}_{12}$ is used in the approximation. Since the non-zero Dirichlet boundary conditions

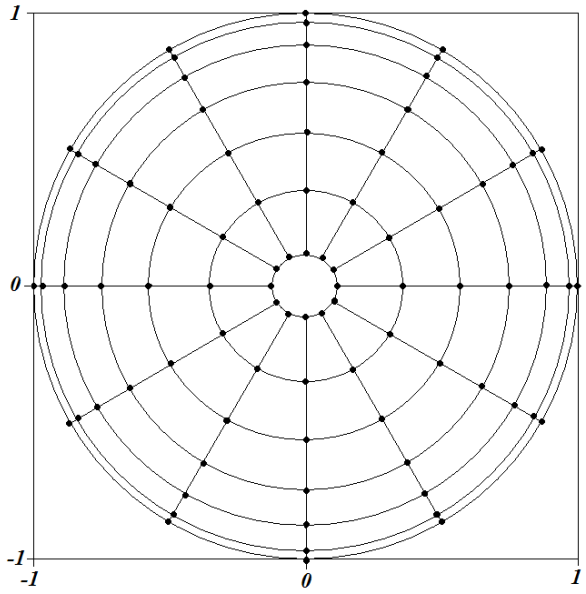

Figure 4.3: Mesh with collocation nodes on the unit disk

are used, values on the boundary are also included in the approximation. Define rectangular $n \times (n+1)$ matrices D_{11} and D_{12}, which are obtained from $\bar{D}_{11}$ and $\bar{D}_{12}$ respectively by excluding the first rows. Also define I_l as identity matrices of size l, and Z_m is the zero matrix of size m. Then the approximation of the operator $\frac{\partial}{\partial R}$ at the interior points of the domain is

$$D_R = D_{11} \otimes I_M + \tilde{D}_{12} \otimes \hat{I}_M, \tag{4.7}$$

here $\hat{I}_M = \begin{bmatrix} Z_m & I_m \\ I_m & Z_m \end{bmatrix}$. The symbol $\otimes$ indicates matrix tensor product defined as

follows: let A and B are two matrices of sizes $n_1 \times m_1$ and $n_2 \times m_2$,then

$$A \otimes B = \begin{bmatrix} a_{11}B & a_{12}B & ... & a_{1m_1}B \\ a_{21}B & a_{22}B & ... & a_{2m_1}B \\ ... & ... & ... & ... \\ a_{n_1 1}B & a_{n_1 2}B & ... & a_{n_1 m_1}B \end{bmatrix}$$

is a $n_1 n_2 \times m_1 m_2$ matrix The approximation of the operator $\frac{\partial}{\partial \theta}$ is

$$D_\theta = [z_n \quad I_n] \otimes DF, \tag{4.8}$$

here $z_n = \underbrace{(0, 0, ..., 0)}_{n}^{T}$ is a zero vector.

Now we can write an approximation of the Laplacian (3.20). The Chebyshev pseudospectral differentiation matrix of the second order is $D^{(2)} = \begin{bmatrix} \bar{D}_{11}^{(2)} & \bar{D}_{12}^{(2)} \\ \bar{D}_{21}^{(2)} & \bar{D}_{22}^{(2)} \end{bmatrix}$. Again we discard $\bar{D}_{21}^{(2)}$ and $\bar{D}_{22}^{(2)}$ and define $D_{11}^{(2)}$, $D_{12}^{(2)}$ as $n \times (n+1)$ matrices, which are obtained from $\bar{D}_{11}^{(2)}$ and $\bar{D}_{12}^{(2)}$ respectively excluding the first rows.

Now the approximation of the operator $L = -\Delta$ at inner points of the grid is

$$\begin{gathered} L = -[g^{RR}](D_{11}^{(2)} \otimes I_M + \tilde{D}_{12}^{(2)} \otimes \hat{I}_M) - 2[g^{R\theta}]D_R(I_{n+1} \otimes DF) - \\ [g^{\theta\theta}]([z_n \quad I_n] \otimes DF^{(2)}) - [g^R]D_R, \end{gathered} \tag{4.9}$$

here $[g^{RR}]$,$[g^{R\theta}]$ and $[g^{\theta\theta}]$ are diagonal matrices, where the diagonal elements are coresponding contravariant metric tensor components (3.19) evaluated at collocation grid points. The diagonal matrix $[g^R]$ is obtained using (3.21) at collocation grid points.

In our problem both unknown functions ω and ϕ have non-zero values on the boundary, hence all expansions include interior and boundary values. As a result

matrix L approximating Laplacian at interior points is an $nM \times dim$ rectangular matrix. For a non-dimpled surface $\epsilon = 0$ the mixed derivative component of the Laplacian is missing and the resulting matrix L has more zero entries than non-zero. For a dimpled surface the resulting matrix is absolutely full (see fig.4.4). That leads to a certain number of problems. Full $O(N^2)$ matrix requires N^2 operations to fill it, and takes a lot of computer memory space for storage, while sparse matrices resulting from low order approximations need only $O(N)$ operations and much less memory space. It should be noted that the size of the grid in pseudospectral applications is comparatively small, because of the high accuracy of the method, and hence the size of the resulting approximation matrix is also much smaller, than those arising in low order methods. To save storage space one can consider a matrix-vector product, then entries of each row of pseudospectral matrix can be computed each time when they are needed. In this case only one row at a time will be stored in memory. This approach is very time consuming in macro-languages like Matlab, because loops are very slow there, and it is better to store the whole matrix, than recompute row each time. But matrix-vector product approach can be efficiently implemented in C++. Also, when Chebyshev and Fourier polynomials are used, the so called FFT technique can reduce the number of operation required in pseudospectral approximation to $N \log N$ [51, 4]. The differential operator $L = -\Delta$ is positive definite (the dot product $((Lx, x) > 0)$, and hence a pseudospectral approximation matrix of this operator L has the same property.

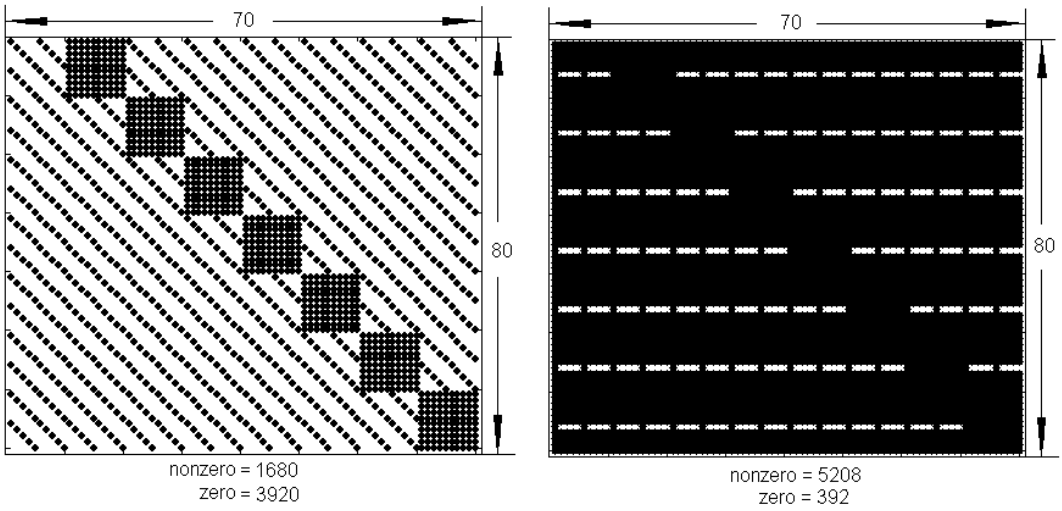

Figure 4.4: Sparsity of the Laplacian matrix for the problem with dimples (right) and without dimples(left)

4.1.3 $f(R)$ and outer collocation grid

Spectral methods based on orthogonal polynomials (Chebyshev) produce computational grids with collocation nodes that are more dense near the boundaries than in the middle of the domain. Although this property works for boundary-layer problems, it may produce some difficulties for problems with large length scales. In the present work the problem is solved on the infinite domain and collocation grid on the physical domain is obtained by mapping from the unit disk. In radial direction on the unit disk the grid spacing is $\frac{1}{O(N^2)}$ near the boundary and $\frac{1}{O(N)}$ near the origin. To obtain grid points on the infinite domain Ω in radial direction we apply the transform $\gamma(\theta)f(R)$, where $f(R)$ maps Chebyshev nodes R_j from the half-interval $[0, 1]$ to the interval $[1; \infty)$ and satisfies the constrains defined in (3.14).

The easiest map $f(R) = \frac{1}{R}$ satisfies (3.14), but gives a very inappropriate node distribution on the infinite domain Ω. It is too dense near the boundary and doesn't

provide enough points away from the boundary (see fig.4.5). One can generalize it to $f(R) = \frac{1}{R^a}$ and change the node distribution varying the parameter a, but the resulting node distribution is still very uneven in the region close to the cylinder (2-3 diameters). To improve the grid we suggest to apply a combination of maps, one will

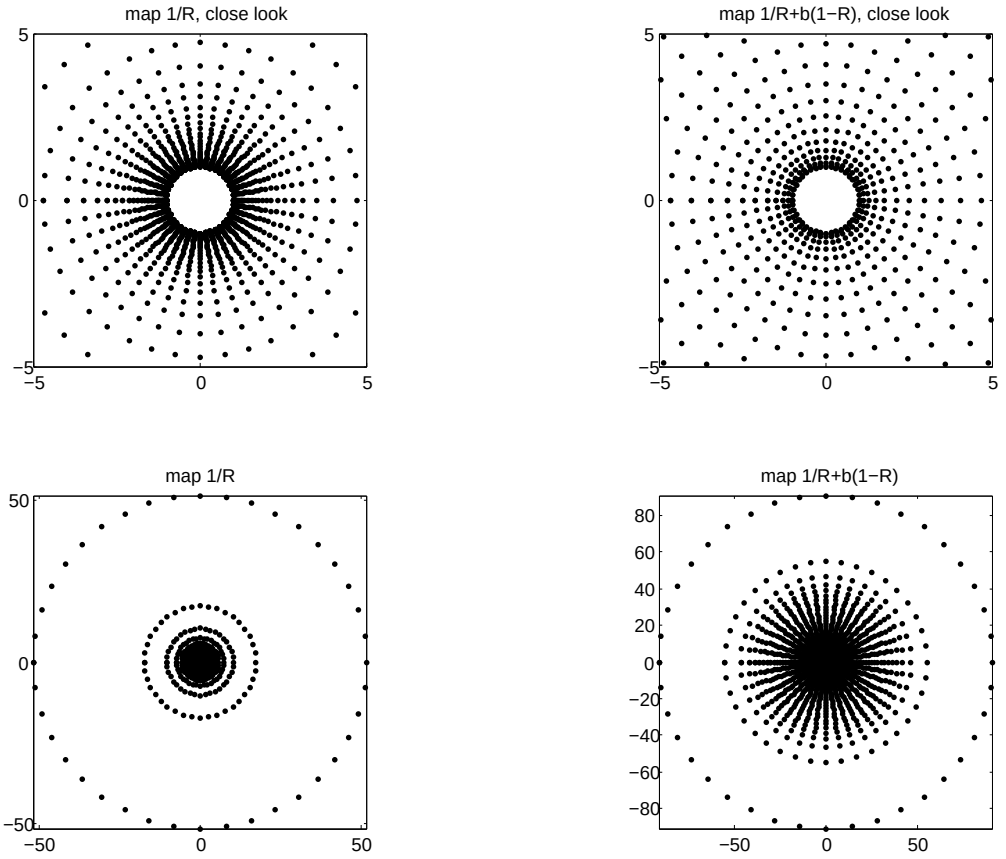

Figure 4.5: The difference in node distribution for maps $f(R) = \frac{1}{R} + b(1-R)$ and $f(R) = \frac{1}{R}$ for the number of grid points $r \times \theta = 41 \times 40$.

provide nodes far from the surface of the cylinder, and another will give a more or less even distribution of grid point near the cylinder. To get a nice spacing between grid point near the cylinder we choose the linear map $b(1-R)$, where the parameter b is approximately equal to the radius of the circular domain which is covered with

grid point, so if we want the region of 30 cylinder diameters being covered with ≈ 60 points, we take $b = 30d = 60$. In present study two maps were tested: one is a combination of of the linear function and a power function:

$$f(R) = R^{-a} + b(1 - R), \qquad a, b > 0. \tag{4.10}$$

and another is a combination of the same linear function and a logarithmic function:

$$f(R) = 1 - a\ln(R) + b(1 - R), \qquad a, b > 0. \tag{4.11}$$

After many experiments we concluded, that the map (4.11) gives more accurate results, than the map (4.10), in both steady and unsteady computations.

4.2 Solution of algebraic linear systems

As result of pseudospectral approximation a system of linear equations with full, non-symmetric and positive definite matrix is obtained:

$$Ax = b.$$

In case with no dimples A is sparse while for a dimpled domain it is full (see fig.4.4). Solution of the system of linear equations with full matrix using direct method such as Gaussian elimination takes at least N^3 iteration for an $N \times N$ matrix. Hence it is sufficient to use an appropriate iterative method, which will give the solution with a minimum number of iterations.

Iterative methods based on Krylov subspace [42] are usually used to solve linear systems of equations. For a given initial guess x_0 m-dimensional Krylov subspaces K_m are subspaces of the form

$$K_m \equiv span\{r_0, Ar_0, A^2r_0, ..., A^{m-1}r_0\}. \tag{4.12}$$

Here $r_0 = b - Ax_0$ is the initial residual. In simple words iterative methods based on (4.12) find an approximation of $A^{-1}b$ by $p(A)b$, where p is a polynomial of degree $\leq m$. Since pseudospectral approximation matrix is non-symmetric, Generalized Minimum Residual Method (GMRES) can be applied. For a given initial vector x_0 and the dimension of the Krylov subspace m, this method minimizes the residual L_2 norm $\| b - Ax \|_2$ over all vectors $x \in x_0 + K_m$.

Spectral matrices based on Fourier-Chebyshev approximation are ill-conditioned, meaning that the condition number $k(A) = \|A\|\|A^{-1}\|$ is large and grows extremely fast with the number of nodes. In numerical linear algebra the condition number is used to analyze convergence of the solution of the linear system, the larger the condition number the slower an iterative method will work. For instance the condition number of the Chebyshev differentiation matrix for the second order problem behaves like $O(N^4)$, where N is the largest degree of polynomial, where for finite differences and finite volumes it is $O(N^2)$. In general it is difficult to give an accurate estimate to the condition number for two and three-dimensional problems. As a result of ill-conditioning it is necessary to use an effective preconditioner in iterative methods, meaning that the preconditioned system

$$B^{-1}Ax = B^{-1}b$$

can be solved instead of the original one. Preconditioner B must be effective in improving the condition number, cheap in computing and storing and easily invertible. Finding the best preconditioning technique for a given linear system of equations is usually an art. Lower order approximations such as finite differences [35, 20] and finite elements [10] are often used as preconditioners for linear systems with pseu-

dospectral matrices. Matrices resulting from low order approximation are sparse and hence don't need a lot of memory.

In the current work the second order finite difference approximations were used for preconditioners. Finite difference matrices are the easiest and cheapest in computing and storing. Inverting a finite difference matrix should be also inexpensive. One of the simplest ways is to apply the incomplete LU factorization [42] of the preconditioner B. Incomplete LU factorization computes sparse lower L and upper U triangular matrices such that the residual $LU - B$ satisfies some constrains. In Matlab built-in incomplete LU factorization and GMRES procedure with preconditioning can be used.

In this project the preconditioner for the spectral approximation matrix of the operator L is needed. Following the same procedure, first we obtain finite difference matrices for the first and second derivative in R and θ direction, then preconditioner can be computed, using tensor product for matrices. The main problem is that the same unevenly spaced grid has to be used for the finite difference approximation in radial direction. For Chebyshev Gauss-Lobatto nodes $R_j = \cos(\frac{\pi j}{N}), j = 0, 1, ..., N$ define $h_{Rj} = R_{j+1} - R_j, j = 0, 1, ..., N$, then centered second order finite difference approximation of the first and second derivatives of some function $f(R)$[4] in radial direction are

$$\frac{\partial f(R_j)}{\partial R} = \left[-\frac{h_{Rj}}{h_{Rj-1}(h_{Rj-1}+h_{Rj})}\right] f_{j-1} - \left[\frac{1}{h_{Rj-1}} - \frac{1}{h_{Rj}}\right] f_j + \left[\frac{h_{Rj-1}}{h_{Rj}(h_{Rj-1}+h_{Rj})}\right] f_{j+1}, \tag{4.13}$$

$$\frac{\partial^2 f(R_j)}{\partial R^2} = \left[\frac{2}{h_{Rj-1}(h_{Rj-1}+h_{Rj})}\right] f_{j-1} - \left[\frac{2}{h_{Rj-1}h_{Rj}}\right] f_j + \left[\frac{2}{h_{Rj}(h_{Rj-1}+h_{Rj})}\right] f_{j+1}. \tag{4.14}$$

Using (4.13-4.14) finite difference matrices D_{fd} and $D_{fd}^{(2)}$ are constructed.

Usual second order finite difference approximations for an evenly Fourier collocation grid $\theta_k = \frac{2\pi k}{M}$ are used to find finite difference matrices DF_{fd} and $DF_{fd}^{(2)}$. Then a finite difference approximation of the operator L is computed similar to (4.9) using finite difference matrices.

4.3 Solution of the steady problem with Newton's method

There are two basic methods used for numerical solutions of steady (flow doesn't change with time) fluid flow problems. The first one involves integrating the time-dependent equations until the steady state solution. Another approach is to solve the steady Navier-Stokes system using a non-linear solver.

The steady Navier-Stokes system is

$$\begin{aligned} L\omega &= ReG(\omega,\phi) \quad in \quad E, \\ L\phi &= \omega \quad in \quad E, \\ \phi &= q(\theta) \quad on \quad \partial E, \\ \tfrac{\partial\phi}{\partial R} &= h(\theta) \quad on \quad \partial E, \end{aligned} \tag{4.15}$$

here $q(\theta) = -\gamma(\theta)\sin\theta$ and $h(\theta) = -f'(1)\gamma(\theta)\sin\theta$.

One popular technique to solve steady Navier-Stokes problems is the Newton's method, which provides quadratic convergence, if an initial guess is close enough to the solution. Hence, it is usually possible to obtain solutions of the discrete equations with relatively small number of non-linear iterations. But there are several difficulties: the initial guess can not be completely arbitrary, it should be close enough to get convergence. Another problem is when the standard Newton's method is

applied, the Jacobian matrix for the linear system of equations must be recomputed at each iteration. Hence in case of pseudospectral approximation the computation and inverting of the Jacobian is especially expensive, because the matrix is full. As an alternative one can implement a modification of the Newton's method, where the Jacobian is computed only once with an initial guess and used in all iterations, but convergence of this method is only linear and it is even more sensitive to the initial guess. Boyd [4] suggests that applying Newton's method directly to a differential equation and then approximating the result with spectral method can slightly reduce the magnitude of the problem with Jacobian.

Let $F(u)$ be a general non-linear differential operator, then $F(u) = 0$ is a system of differential equations, that has to be solved. Newton's method is based on the generalized Taylor's series of a non-linear operator $F(u)$:

$$F(u + \delta u) = F(u) + F_u(u)\delta u + O(\delta u^2) = 0, \tag{4.16}$$

where $F_u(u)$ is the Frecher differential of the non-linear operator, defined by

$$F_u(u)\delta u = \lim_{\epsilon \to 0} \frac{F(u + \epsilon \delta u) - F(u)}{\epsilon}. \tag{4.17}$$

From the Taylor's series expansions (4.16)

$$\delta u = -F_u^{-1}(u)F(u) + F_u^{-1}(u)O(\delta u^2)$$

and $u + \delta u$ is an approximation of the solution of $F(u) = 0$. Starting with an initial guess u^0 the Newton's iteration

$$\delta u^n = -F_u^{-1}(u^n)F(u^n), \tag{4.18}$$

$$u^{n+1} = u^n + \delta u^n \tag{4.19}$$

is performed until $\|\delta u^n\| < tol$, where tol - is a small enough tolerance.

Here we implement the full Newton's method to the steady non-linear problem (4.15). First we define the non-linear differential operator

$$F(\omega, \phi) = \begin{bmatrix} L\omega - ReG(\omega, \phi) \\ L\phi - \omega \end{bmatrix} \tag{4.20}$$

Now $F(\omega, \phi) = 0$ is the system of differential equations in (4.15). Taking the derivative of the operator $F(\omega, \phi)$ we get

$$J_F(\omega, \phi) = \begin{bmatrix} L - ReG_\omega(\phi) & -ReG_\phi(\omega) \\ -I & L \end{bmatrix} \tag{4.21}$$

Here I is an identity operator and

$$G_\omega(\phi) = \left(\frac{1}{|J|}\frac{\partial \phi}{\partial R} + \frac{J_{21}}{|J|}\right)\frac{\partial}{\partial \theta} - \left(\frac{1}{|J|}\frac{\partial \phi}{\partial \theta} + \frac{J_{22}}{|J|}\right)\frac{\partial}{\partial R} \tag{4.22}$$

$$G_\phi(\omega) = \frac{1}{|J|}\left(\frac{\partial \omega}{\partial \theta}\frac{\partial}{\partial R} - \frac{\partial \omega}{\partial R}\frac{\partial}{\partial \theta}\right) \tag{4.23}$$

Since the initial guess (ω^0, ϕ^0) can be far from the solution, the Newton step $S_n = -J_F(\omega^n, \phi^n)^{-1}F(\omega^n, \phi^n)$ can be large and method may diverge. An alternative way is to use the Newton's method with backtracking [24]:

$$\delta[\omega^n, \phi^n]^T = \lambda_n S_n \tag{4.24}$$

here $\delta[\omega^n, \phi^n]^T = [\omega^{n+1}, \phi^{n+1}]^T - [\omega^n, \phi^n]^T$. The parameter $0 < \lambda_n \leqslant 1$ is initially set to 1 and its value decreases by the half until the condition

$$\|F((\omega^n, \phi^n)^T + \lambda_n S_n)\|_2^2 < \|F(\omega^n, \phi^n)\|_2^2 + \alpha\lambda_n \nabla F(\omega^n, \phi^n)\|_2^2 \cdot S_n \tag{4.25}$$

is satisfied for some small $\alpha \sim 10^{-3} - 10^{-4}$. So, if the parameter $\lambda_n = 1$ we are close to the solution and if $\lambda_n << 1$ we are far from it. Note, that

$$\nabla\|F(\omega^n, \phi^n)\|_2^2 \cdot S_n = 2F(\omega^n, \phi^n)^T \nabla F(\omega^n, \phi^n)(-\nabla F(\omega^n, \phi^n)^{-1}F(\omega^n, \phi^n)) =$$

$$-2F(\omega^n,\phi^n)^T F(\omega^n,\phi^n) = -2\|F(\omega^n,\phi^n)\|_2^2 \leqslant 0.$$

Hence we can rewrite (4.25)

$$\|F((\omega^n,\phi^n)^T + \lambda_n S_n)\|_2^2 < (1-2\alpha\lambda_n)\|F(\omega^n,\phi^n)\|_2^2 \tag{4.26}$$

To implement boundary conditions the Newton's iteration (4.24), we must take the initial guess, that satisfies boundary conditions. Hence we should provide ϕ^0, that satisfies two boundary conditions in (4.15): one is a Dirichlet and another is Neuman condition. For the Dirichlet condition we take $\delta\phi^n = 0$ and for the Neuman $\frac{\partial\delta\phi^n}{\partial R} = 0$.

To define the linear system of equations, resulting from the pseudospectral approximation of the Newton's iteration (4.24) we represent unknown function as $\omega = (\omega_b, \omega_{in})^T$ and $\phi = (\phi_b, \phi_{in})^T$, where indices "$b$" and "$in$" denote values at boundary and inner collocation points respectively. Then the pseudospectral approximation of the differential operator (4.20) is

$$F = \begin{bmatrix} D_{Rb}\phi - h(\theta_b) \\ L\omega - ReG(\omega,\phi) \\ \phi_b - q(\theta_b) \\ L\phi - \omega_{in} \end{bmatrix} \tag{4.27}$$

here D_{Rb} is a pseudospectral approximation matrix of the operator $\frac{\partial}{\partial R}$ at boundary collocation points, L is a pseudospectral matrix defined in (4.9) for inner points and $G(\omega,\phi)$ is a pseudospectral approximation of the nonlinear term (3.26) at inner points.

The approximation of the Jacobian (4.21) is

$$J_F = \left[\begin{array}{c|c} Z_{M,dim} & D_{Rb} \\ L - ReG_\omega(\phi) & -ReG_\phi(\omega) \\ \hline Z_{M,dim} & I_{M,dim} \\ -I_{nM,dim} & L \end{array}\right] \tag{4.28}$$

where $Z_{M,dim}$ is a rectangular $M \times dim$ zero matrix, $I_{M,dim}$ is a matrix that consists of first M rows of the identity matrix of size dim, and $I_{nM,dim}$ consists of last nM rows of the same identity matrix, $G_\omega(\phi)$ and $G_\phi(\omega)$ are rectangular matrices, resulting from the pseudospectral approximation of operators (4.22-4.23), and recomputed at each Newton step with new ϕ and ω. At each Newton step n the following problem is solved

$$\begin{gathered} J_F^n \left[\begin{array}{c} d\omega^n \\ d\phi^n \end{array}\right] = -\lambda_n F^n \\ \omega^{n+1} = \omega^n + d\omega, \quad \phi^{n+1} = \phi^n + d\phi \end{gathered} \tag{4.29}$$

until the sufficient condition (4.26) is satisfied.

Damped Newton's algorithm with backtracking:

Let $n = 0$ and the initial guess is (ω^0, ϕ^0)

- compute $F_n = F(\omega^n, \phi^n)$ by (4.27);
- WHILE $\|F_n\|_2 \geqslant \beta$:
  1. compute the Jacobian $J_F^n = J_F(\omega^n, \phi^n)$ by (4.28) (note, that only G_ω and G_ϕ in (4.28) should be recomputed at each iteration);
  2. take $\lambda_n = 1$;

3. solve (4.29);
4. compute $F_{n+1} = F(\omega^{n+1}, \phi^{n+1})$ by (4.27);
5. WHILE $\|F_{n+1}\|_2^2 \geqslant (1 - 2\alpha\lambda_n)\|F_n\|_2^2$
   - take $\lambda_n = \lambda_n/2$;
   - solve (4.29);
   - compute $F_{n+1} = F(\omega^{n+1}, \phi^{n+1})$ by (4.27);

   END WHILE;
6. $n = n + 1$;

END WHILE.

As we increase the Reynolds number ($Re > 30$) the Newton's method with backtracking often diverges, unless a very fine grid is taken or the initial guess is very close to the solution. Since taking a large grid is very expensive, so the best approach here is to define a good initial guess. The solution for the lower Re can be used as an initial guess. We define the initial guess by running several iterations of the time code, it is very inexpensive, because the semi-implicit time iteration takes much less time then Newton iteration.

4.4 Solution of the unsteady problem

4.4.1 Time discretization

The time discretization is usually based on finite difference methods. Hence, the high order accuracy of spectral methods is restricted by the lower accuracy of the

time integration. Very few attempts are made to derive spectral approximations in time [18], and an obvious reason is that the computational cost, including memory and time, is too large. To preserve the high accuracy of the spectral method it is recommended, that at least a third order time scheme is used especially for highly unsteady flows [37].

Solution of the second order time-dependent problems with spectral method, using an explicit scheme, requires a very small time-step for stability ($\Delta t \sim \frac{Re}{N^4}$, where N is the highest degree of polynomial), otherwise method will diverge. On the other hand fully implicit methods have better stability properties. But they are too expensive, because a set of non-linear equations has to be solved at each time step. Implicit methods are usually applied for flows with variable density ρ (compressible flows) or viscosity μ. When the coefficients of the linear operator (here Laplacian) are time independent the semi-implicit are generally applied [37].

Semi–implicit methods, where diffusive term (Laplacian) of the vorticity equation is treated implicitly and the non-linear term is treated explicitly, are a good choice for laminar problems. Using semi-implicit methods overcomes the problem of severe restriction on the time-step which occurs in explicite methods, where the influence of the diffusive term is sufficient. In this project we apply Adams–Bashforth/Backward–Differentiation method [37]. Consider the vorticity equation:

$$\frac{\partial \omega}{\partial t} + \frac{1}{Re} L\omega = G(\omega, \phi) \tag{4.30}$$

Linear part of the equation (4.30) is treated implicitly. An implicit k-th order Backward-Differentiation schemes are used for the discretization of time derivative

of the vorticity:

$$\frac{\partial \omega}{\partial t} = \frac{1}{\Delta t} \sum_{j=0}^{k} a_j \omega^{l+1-j}$$

Explicit Adams-Bashforth schemes are used for time discretization of the non-linear part of the Navier-Stokes system. The application of the general AB/BDIk to equation (4.30) gives:

$$\frac{1}{\Delta t} \sum_{j=0}^{k} a_j \omega^{l+1-j} + \frac{1}{Re} L\omega^{l+1} = \sum_{j=0}^{k-1} b_j G(\omega^{l-j}, \phi^{l-j}) \tag{4.31}$$

The table of coefficients a_j and b_j for 2,3,4 order AB/BDI schemes can be found in Peyret's book (see table 4.4 in [37]).

Let $f^{l+1} = \sum_{j=0}^{k-1} b_j G(\omega^{l-j}, \phi^{l-j}) - \frac{1}{\Delta t} \sum_{j=1}^{k} a_j \omega^{l+1-j}$, then the following linear problem has to be solved at each time level:

$$\left(\frac{a_0}{\Delta t} + \frac{1}{Re} L\right) \omega^{l+1} = f^{l+1} \quad in \quad E \tag{4.32}$$

$$L\phi^{l+1} = \omega^{l+1} \quad in \quad E \tag{4.33}$$

$$\phi^{l+1} = q(\theta) \quad on \quad \partial E \tag{4.34}$$

$$\frac{\partial \phi^{l+1}}{\partial R} = h(\theta) \quad on \quad \partial E \tag{4.35}$$

Equations (4.32) for the second,third and fourth order approximations in time are:

k=2:

$$\left(\frac{3}{2\Delta t} + \frac{1}{Re} L\right) \omega^{l+1} = 2G(\phi^l, \omega^l) - G(\phi^{l-1,\omega^{l-1}}) + \frac{2}{\Delta t}\omega^l - \frac{1}{2\Delta t}\omega^{l-1}$$

k=3:

$$\left(\frac{11}{6\Delta t} + \frac{1}{Re} L\right) \omega^{l+1} = 3G(\phi^l, \omega^l) - 3G(\phi^{l-1}, \omega^{l-1}) + G(\phi^{l-2}, \omega^{l-2}) + \frac{3}{\Delta t}\omega^l -$$

$$-\frac{3}{2\Delta t}\omega^{l-1}+\frac{1}{3\Delta t}\omega^{l-2}$$

k=4:

$$\left(\frac{25}{12\Delta t}+\frac{1}{Re}L\right)\omega^{l+1}=4G(\omega^{l},\phi^{l})-6G(\omega^{l-1},\phi^{l-1})+4G(\omega^{l-2},\phi^{l-2})-$$

$$-G(\omega^{l-3},\phi^{l-3})-\frac{1}{\Delta t}\left(-4\omega^{l}+3\omega^{l-1}-\frac{4}{3}\omega^{l-2}+\frac{1}{4}\omega^{l-3}\right)$$

Although all 3 time schemes are implemented, most numerical experiments were carried out with AB/BDI3. It means that we use a high order approximation in space and third order in time. It allows as to get the solution for the flow past smooth cylinder with error of accuracy $\sim 10^{-4}$ on the 41×40 grid for the time step $0.01\leq\Delta t\leq 0.025$.

4.4.2 Influence matrix method

The vorticity-streamfunction formulation of the fluid flow problem provides two no-slip boundary conditions for the streamfunction, but none for the vorticity. In applications of spectral methods to the Navier-Stokes problems the influence matrix method is commonly used to impose boundary conditions for the vorticity [50, 7, 49] or the pressure [28, 51] implicitly.

When the influence matrix method is applied, the solution $(\omega,\phi)=(\omega^{l+1},\phi^{l+1})$ of the discrete problem

$$A\omega=0 \quad in \quad E_{N,M} \tag{4.36}$$

$$L\phi=\omega \quad in \quad E_{N,M} \tag{4.37}$$

$$\phi|_{(1,\theta_j)}=q(\theta_j) \tag{4.38}$$

$$\frac{\partial\phi}{\partial R}|_{(1,\theta_j)}=h(\theta_j) \tag{4.39}$$

is decomposed by

$$\omega = \tilde{\omega} + \sum_{k=1}^{M} \xi_k \omega_k, \quad \phi = \tilde{\phi} + \sum_{k=1}^{M} \xi_k \phi_k \tag{4.40}$$

Here $(\tilde{\omega}, \tilde{\phi})$ is the solution of the problem:

$$\begin{aligned} A\tilde{\omega} &= f \quad in \quad E_{N,M} \\ L\tilde{\phi} &= \tilde{\omega} \quad in \quad E_{N,M} \\ \tilde{\omega}|_{(1,\theta_j)} &= 0 \\ \tilde{\phi}|_{(1,\theta_j)} &= q(\theta_j) \end{aligned} \tag{4.41}$$

and (ω_k, ϕ_k) are solutions of problems:

$$\begin{aligned} A\omega_k &= 0 \quad in \quad E_{N,M} \\ L\phi_k &= \omega_k \quad in \quad E_{N,M} \\ \omega_k|_{(1,\theta_j)} &= \delta_{kj} \\ \phi_k|_{(1,\theta_j)} &= 0 \end{aligned} \tag{4.42}$$

One can easily show that the final solution (4.40) satisfies the problem (4.36-4.39)

$$A\omega = A\tilde{\omega} - \sum_{k=1}^{M} \xi_k A\omega_k = f$$

$$L\phi = L\tilde{\phi} - \sum_{k=1}^{M} \xi_k L\phi_k = \tilde{\omega} + \sum_{k=1}^{M} \xi_k \omega_k = \omega$$

$$\phi|_{(1,\theta_j)} = \tilde{\phi}|_{(1,\theta_j)} + \sum_{k=1}^{M} \xi_k \phi_k|_{(1,\theta_j)} = q(\theta_j)$$

and $\omega|_{(1,\theta_j)} = \tilde{\omega}|_{(1,\theta_j)} + \sum_{k=1}^{M} \xi_k \omega_k|_{(1,\theta_j)} = \xi_j$. The influence of the boundary vorticity is represented by the influence matrix. Solving the linear system with the influence matrix the values ξ_j are determined. To construct the influence matrix the second boundary condition for the stream-function (4.39) is used:

$$\frac{\partial \tilde{\phi}}{\partial R}|_{(1,\theta_j)} + \sum_{k=1}^{M} \frac{\partial \phi_k}{\partial R}|_{(1,\theta_j)} \xi_k = h(\theta_j)$$

or

$$W\Xi = g \tag{4.43}$$

Where $\Xi = (\xi_{1,...,}\xi_M)^T$, $g = (h(\theta_1) - \frac{\partial\tilde{\phi}}{\partial R}|_{(1,\theta_1)}, ..., h(\theta_M) - \frac{\partial\tilde{\phi}}{\partial R}|_{(1,\theta_M)})^T$, and W is the influence matrix with entries

$$w_{j,k} = \frac{\partial\phi_k}{\partial R}|_{(1,\theta_j)} \tag{4.44}$$

Note that the system (4.36-4.39) is solved only once at the beginning, and the influence matrix is computed by (4.44) and used to update the boundary values of ω by (4.43). When the influence matrix method for the time problem was implemented, it turned out to be very slow for our computation, especially for the case with dimpled geometry. The reasons are, that in addition to storing the inverted influence matrix and solving (4.43), we need either to store matrices of solutions of homogenous problem (4.42) or recompute the system (4.41) with boundary conditions for the vorticity, obtained from (4.43). To speed up the solver, the coupled system of equations involving two boundary conditions for ϕ is solved instead.

4.4.3 An alternative solution of the discretized problem

When the influence matrix method is applied to the unsteady problem, discretized by semi-implicit AB/BDIk, the vorticity and streamfunction equations are solved separately one after another, the solution of the same problem by including both no-slip conditions as described for the steady problem in sec. 4.3 takes both equations into the same algebraic linear system of equations.

Let $\omega = (\omega_b, \omega_{in})^T$ and $\phi = (\phi_b, \phi_{in})^T$, where indices "$b$" and "$in$" denote values at boundary and inner collocation points respectively and L is a pseudospectral

approximation operator $-\Delta$(4.9). Consider the pseudospectral approximation of the system (4.32):

$$\left[\begin{array}{c|c} Z_{M,dim} & D_{Rb} \\ D_t + \frac{1}{Re}L & Z_{nM,dim} \\ \hline Z_{M,dim} & I_{M,dim} \\ -I_{nM,dim} & L \end{array}\right] \left[\begin{array}{c} \omega_b \\ \omega_{in} \\ \hline \phi_b \\ \phi_{in} \end{array}\right] = \left[\begin{array}{c} h(\theta_b) \\ f^{l+1} \\ \hline q(\theta_b) \\ {}_{nM} \end{array}\right] \tag{4.45}$$

First rows of upper and lower blocks of the system (4.45) represent the approximation of two no-slip boundary condition, second rows are approximations of time discretized equations from (4.32). As in sec.4.3, $Z_{M,dim}$ is a rectangular $M \times dim$ zero matrix, $I_{M,dim}$ is a matrix that consists of first M rows of the identity matrix of size dim, and $I_{nM,dim}$ consists of last nM rows of the same identity matrix. Also $D_t = \frac{a_0}{\Delta t} I_{nM,dim}$ is a rectangular matrix, $f^{l+1} = \sum_{j=0}^{k-1} b_j G(\omega^{l-j}, \phi^{l-j}) - \frac{1}{\Delta t}\sum_{j=1}^{k} a_j \omega_{in}^{l+1-j}$, where $G(\omega^{l-j}, \phi^{l-j})$ are pseudospectral approximations of the non-linear operator (3.26) at inner collocation points using computed values of ω^{l-j} and ϕ^{l-j} from k previous time steps, z_{nM} is a zero vector of size nM.

Solving the algebraic linear system of equations (4.45), using iterative solver GMRES with finite difference preconditioner, at each time level l, the solution at each time $l\Delta t$ is obtained. Since the final algebraic system of equations includes boundary values, the unknown vorticity on the boundary ω_b is updated automatically with each solution of (4.45).

Chapter 5

Numerical experiments

Numerical algorithms for steady and unsteady flow simulations were implemented in Matlab. Because the flow past circular cylinder has a long history of experimental and numerical studies [9, 11, 13, 45, 48, 54], it was used as a benchmark to test our method for the steady or unsteady flow simulations.

In this chapter we present results of simulations of flows past cylinders with different number of dimples. The major reason for numerical solutions of the steady flow problem is to obtain the information on the nature of theoretical study as $Re \rightarrow \infty$. Solutions, obtained by integrating the steady system (4.15), represent symmetric flow with two steady vortices behind the cylinder even for Re, at which experimental and unsteady flow simulations perform the Karman vortex street [11, 13, 45]. Hence, to determine values of Re at which flows past dimpled cylinders become periodic, we use the unsteady solver.

In our experiments we fix parameters a and b of the map (4.11). Since parameter a contributes to the node distribution far from the cylinder we choose different value for two flow regimes: $a = 2$ for the steady simulations and $a = 1$ for the unsteady flow simulations. Parameter provides nearly uniform node distribution in a region around a cylinder and is equal to 60 in all computations.

5.1 Steady flow simulations

5.1.1 Spatial accuracy

To demonstrate the high order of spatial approximation a series of numerical experiments for the flow past a smooth cylinder at $Re = 10$ were carried out. Convergence in radial and angular direction were studied separately.

To show the convergence in angular direction the number of Chebyshev modes and their distribution after the mapping (4.11) are fixed. We take the number of Chebyshev nodes $n + 1 = 41$ and the number of Fourier nodes θ_k, $k = 0, ..., 2m$ is varied with $32 \leq m \leq 120$. Simulations were carried out for the $Re = 10$ and the vorticity at two distinct collocation points from the close to the cylinder region was evaluated.

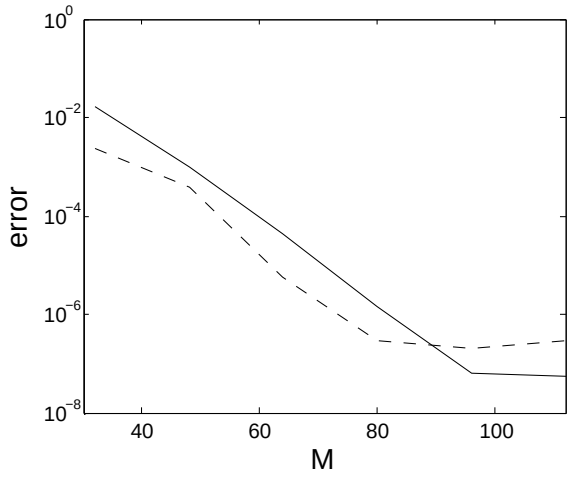

– – – error at the point $\left(f(cos(2\pi/81), \frac{\pi}{8}\right)$;
——— error at the point $\left(f(cos(5\pi/81), -\frac{\pi}{4}\right)$

Figure 5.1: Angular convergence of relative error $|\omega_{120} - \omega_M|/|\omega_{120}|$ on the grid $r \times \theta = 41 \times M$ for the flow at Re=10.

To show the convergence in radial direction we fix the nodes distribution in the angular direction at $M = 60$. Again we consider the flow at $Re = 10$. Since the distribution of Chebyshev points is uneven and their positions are different for distinct n unless doubled n is taken for each experiment. Since we are using the pseudospectral method where functions are approximated using Fourier and Chebyshev expansions a function at any $\bar{R}$ can be easily computed using its values at collocation points:

$$u(\bar{R}, \theta_k) = \sum_{i=0}^{n} \left[q_i(\bar{R}) u(R_i, \theta_k) + q_{N-i}(\bar{R}) u(R_i, \theta_{k+m}) \right], \tag{5.1}$$

where q_i are Lagrange polynomial for the set of Chebyshev collocation points $\{R_i\}_{i=0}^{N}$ defined by (4.2) at which $g_i(R_k) = \delta_{ki}$ and $m = M/2$.

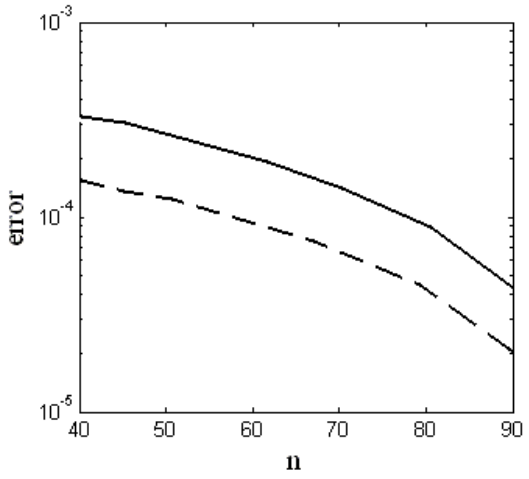

– – – $error_\omega$ along the coordinate line with $\bar{R} = R_9 = cos(10\pi/201)$;
——— $error_\phi$ along the coordinate line with $\bar{R} = R_{19} = cos(20\pi/201)$.

Figure 5.2: Radial convergence of relative errors $|u_{100} - u_n|/|u_{100}|$, $u = \omega, \phi$ on the grid $r \times \theta = (n+1) \times 60$ for the steady flow at Re=10.

Series of simulations for $40 \leq n \leq 100$ are performed. Solution on the mesh $(n+1) \times M = 101 \times 60$ is taken as a reference solution. First we evaluate ω and ϕ

along some fixed coordinate lines with $\bar{R} = R_k$. For $40 \leq n \leq 80$ values of ω and ϕ are interpolated to points on the coordinate line $\bar{R}$ using (5.1) and the relative error with reference solution is computed.

Results of numerical experiments show nice convergence properties of pseudospectral approximation. From the experiments we conclude that the coarsest mesh providing the accurate result for the steady flow problem for $Re \leq 20$ is 41×40. For larger Re ($20 < Re \leq 40$) one should take a mesh of size 61×60 as a coarsest. For the flow with zero Re (linear problem) the accuracy of the solution is $\sim 10^{-14}$ on a mesh of any size $\geq 21 \times 20$.

5.1.2 Steady flow past a smooth cylinder

As a benchmark of the steady solver, simulated flows were compared with experimental and numerical results reported in the literature [9, 11, 13, 36, 40, 45, 48]. For the steady fluid flow past a circular cylinder, the characteristic quantities usually include the drag coefficient C_D, the separation angle θ_s and the wake length L_w. Drag is computed by (3.46) using trapezoidal rule. The reason to use trapezoidal rule and not a higher order method, like say Simpson's rule, is because the integrated functions are smooth and periodic. For smooth periodic functions trapezoidal rule is spectrally accurate, so there is no need in higher order ones [53]. As it was mentioned in sec.3.3 the separation angle θ_s can be determined from zero-vorticity at the surface of the cylinder. The wake length, L_w is the distance between the rear of the cylinder to the end of the separated region. The most accurate way is to use values of the x-component of the velocity u along the x-coordinate line. The x value, at which u changes its sign from negative to positive, gives the end point of the wake

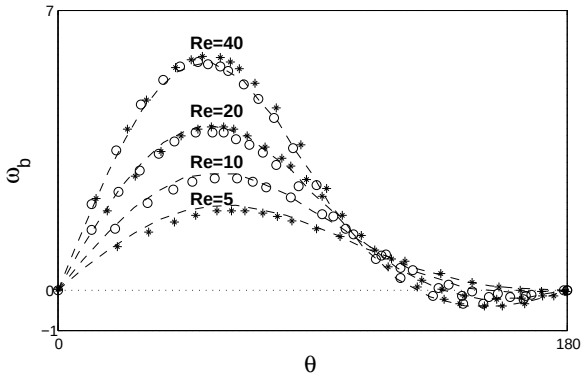

- - – present study; o – Fornberg [13];
$*$ – Dennis & Chang [11].

Figure 5.3: Vorticity on the boundary for different Re.

x_s, then $L_w = x_s - d/2$, where d is the cylinder diameter.

For small Reynolds values between 0 and 20 it is enough to take a grid of size 31×30 the computational grid to get convergence. As we increase Re number the grid required for convergence becomes larger. In present simulations largest grid size is 81×80, that is more than enough for steady flow computations for $0 < Re < 50$.

The variation of the vorticity on the cylinder surface as a function of Re is shown on fig.5.3. Results for $Re = 5, 10, 20, 40$ agree with those given by Dennis and Chang [11] and Fornberg [13] (see fig.5.3).

As a demonstration of how the steady flow changes with Reynolds number, we show numerical results for $Re = 10, 20, 40$ on fig.5.4. Results indicate that the wake behind the cylinder (see. fig.5.5) increases linearly with Re. Applying least square fitting to numerical results of the wake length, we find the straight line equation,

which has a form:

$$L_{smooth}(Re) = 0.0672Re - 0.4091$$

The difference between the straight line and numerical data is shown on fig.5.6. The decaying of the drag coefficient C_D and the grows of the angle of separation are shown on fig.5.1 and fig.5.7 respectively. These results have a good agreement with results of other authors.

	$Re = 20$			$Re = 40$		
	C_D	θ_S	L_w/d	C_D	θ_S	L_w/d
Tritton [48] (exp)	2.22	-	-	1.48	-	-
Coutanceau & Bouard[9] (exp)	-	44.8	0.93	-	53.5	2.13
Takami & Keller[45] (num)	2.0027	43.65	0.935	1.5359	53.55	2.325
Dennis & Chang [11] (num)	2.045	43.7	0.94	1.522	53.8	2.345
Fornberg [13] (num)	2.0001	-	0.91	1.4980	-	2.24
Ramšak et al. [40] (num) N(bound. elem.)=112.500	2.14	43	0.94	1.59	53.3	2.27
Pacheco et al. [36] (num)	2.08	-	0.91	1.53	-	2.28
current study	2.1126	43.27	0.9236	1.5119	53.1	2.24

Table 5.1: Experimental and numerical results of the drag coefficient C_D, separation angle θ_S and the ratio of the wake length L_w over the diameter d for Re=20,40

For flows at $Re \leq 40$ the same results are obtained by running the unsteady code with the same parameters (grid size and coefficients in the transformation $f(R)$).

5.1.3 Steady flow past a dimpled cylinder

Here we present several experiments for dimpled cylinder. In order to have enough memory space to store dense matrices experiments were carried for the number of

Re=10. Grid size $R \times \theta = 50 \times 60$.

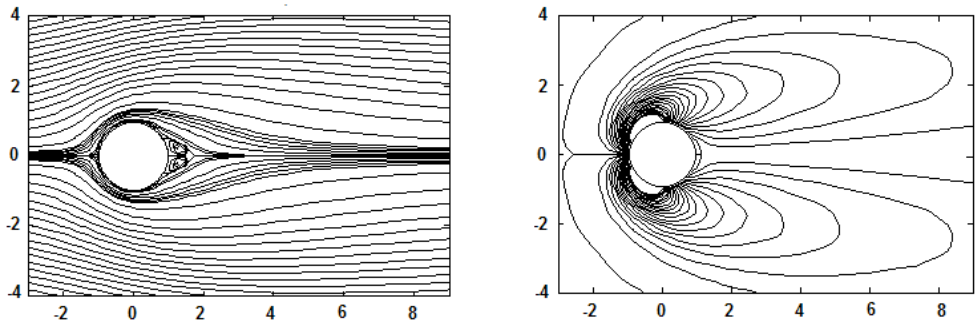

Re=20. Grid size $R \times \theta = 60 \times 60$.

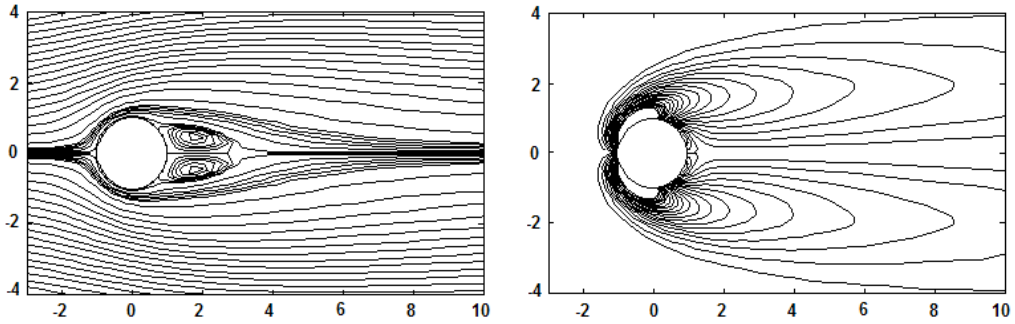

Re=40. Grid size $R \times \theta = 60 \times 80$.

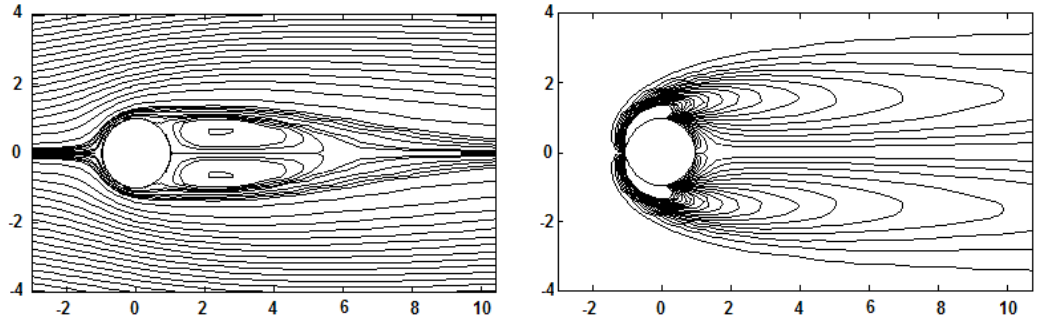

Streamlines (left) and vorticity (right) contours at Re=10,20,40. Stream contours are -2: 0.2: 2, -0.1: 0.02: 0.1, and -0.002: 0.0002: 0.002(Re=10), -0.01: 0.002: 0.01(Re=20), -0.016: 0.008: 0.016(Re=40). Vorticity contours are -2: 0.1: 2 for all cases.

Figure 5.4: Steady flow past a smooth cylinder.

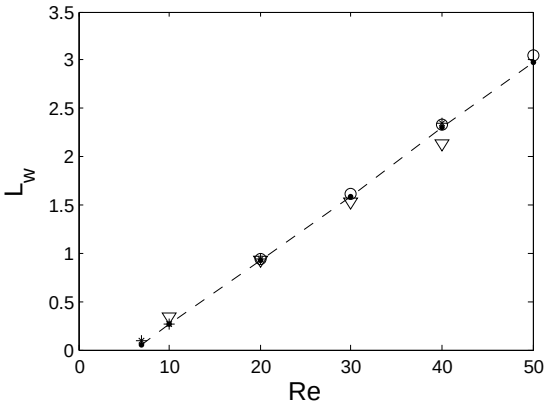

$- \cdot -$ - present study;
$*$ - Dennis & Chang [11]; ∇ - Coutanceau & Bouard[9];
O - Takami & Keller[45].

Figure 5.5: The wake length as a function of Re for a smooth cylinder.

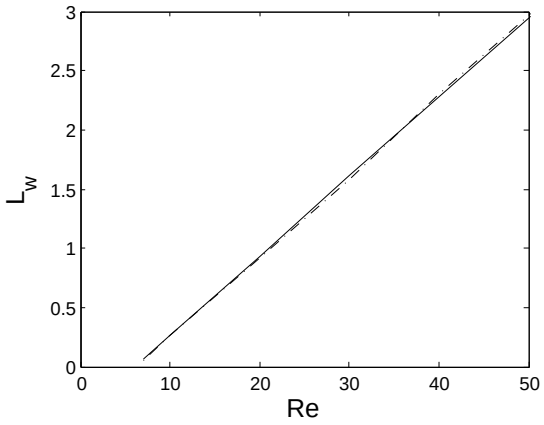

$- \cdot -$ - numerical data;
$-$ - fitting line L_{ls} for numerical data

Figure 5.6: Numerical results for the wake length vs the linear function, obtained using least squares for the numerical data, for the steady flow past a smooth cylinder.

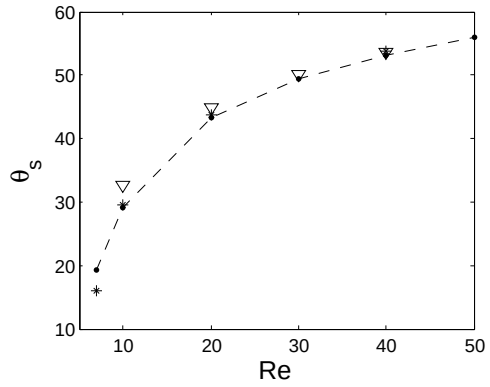

$-\cdot-$ - present study; $*$ - Dennis & Chang [11];
∇ - Coutanceau & Bouard[9].

Figure 5.7: The separation angle as a function of Re for the steady flow past a smooth cylinder.

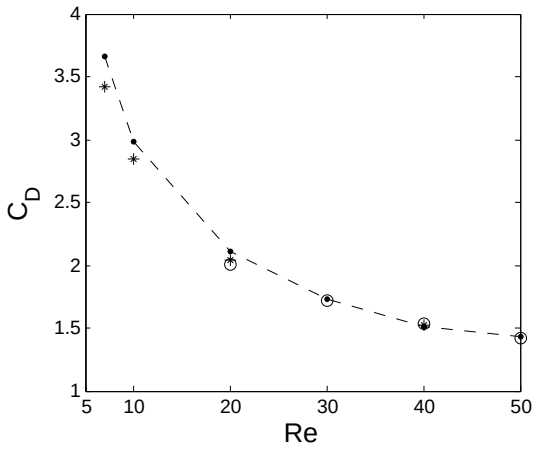

$-\cdot-$ - present study; $*$ - Dennis & Chang [11];
O - Takami & Keller[45].

Figure 5.8: The drag coefficient as a function of Re for the steady flow past a smooth cylinder.

dimples $4 \leq c \leq 12$. For the larger amount of dimples the grid size has to be large enough to handle small scale vortices, which are formed by small size dimples. It was observed that the number of grid point per dimple in angular direction M has to be 5 or 6 in order to obtain reasonable results with good resolution of the flow.

First we perform flow pictures at fixed $Re = 10$ for different number of dimples c with the size of dimples, computed by

$$\epsilon = \frac{\pi}{4c}$$

which means the depth of each dimple ($= 2\epsilon$) is 2 times smaller then its width ($= \frac{\pi}{c}$). Resulting flow picture are presented on fig.5.9.

To study the influence of dimples on a steady state flow characteristics we performed series of computations: a. for $c = 4$ and b. for $c = 8$, with $\epsilon = \frac{\pi}{c^2}$ in both cases. Varying the $10 \leq Re \leq 40$ we recorded the drag coefficient C_D, the separation angle θ_s and the wake length L_w (see fig. 5.10, 5.11 an 5.12).

Applying least square fitting to numerical results for the wake length behind dimpled cylinders, we find the straight line equations. The line for the cylinder with 4 dimples is

$$L_{c=4}(Re) = 0.1070Re - 0.4499,$$

and for for the cylinder with 8 dimples it has the following equation

$$L_{c=8}(Re) = 0.0645Re - 0.3167$$

c=4:

Streamfunction Vorticity

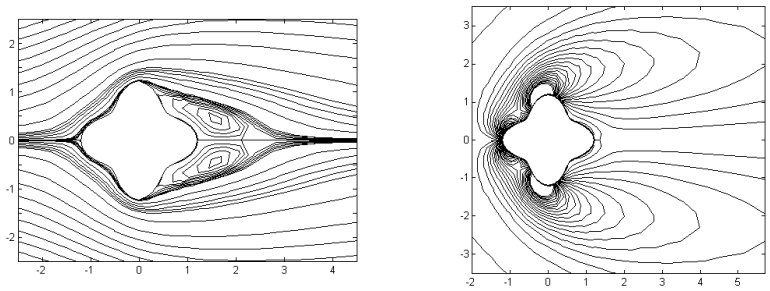

c=8:

Streamfunction Vorticity

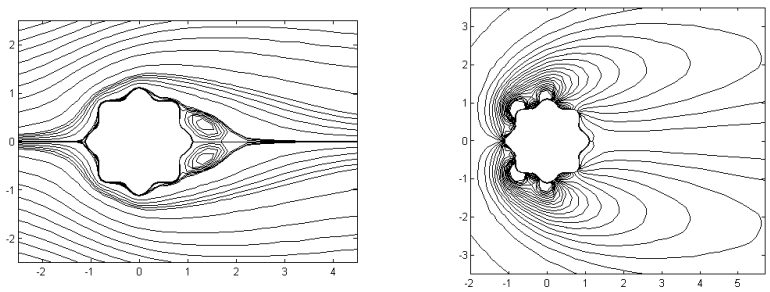

c=12:

Streamfunction Vorticity

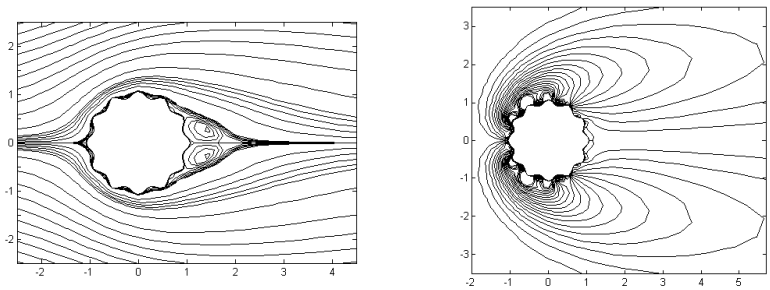

Figure 5.9: The flow past dimpled cylinders with various number of dimples c and size of dimples $\epsilon = \frac{\pi}{4c}$ at Re=10.

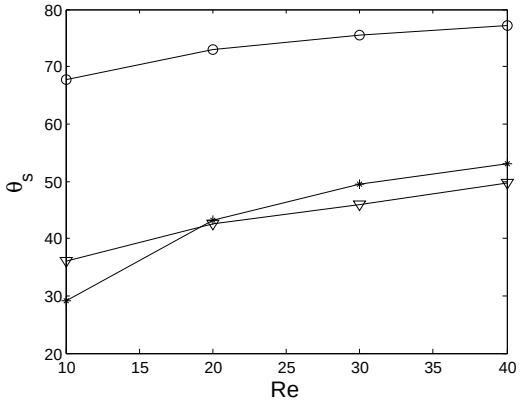

-∗- -smooth cylinder;
-O- - test a;
-∇- - test b.

Figure 5.10: The separation angle of the steady flow past smooth and dimpled cylinders.

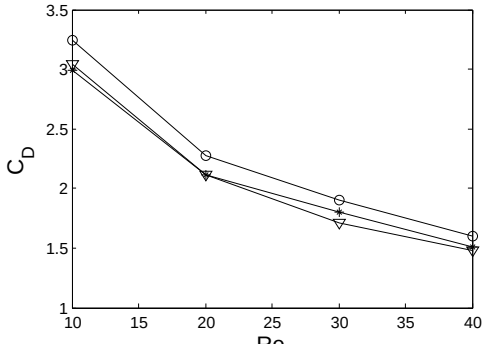

-∗- -smooth cylinder;
-O- - test a;
-∇- - test b.

Figure 5.11: The drag coefficient of the steady flow past smooth and dimpled cylinders.

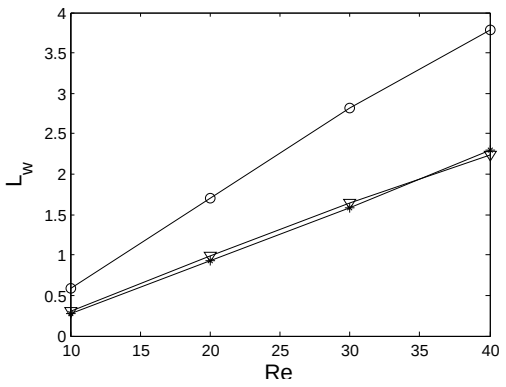

-∗- -smooth cylinder;
-O- - test a;
-∇- - test b.

Figure 5.12: The wake length of the steady flow past smooth and dimpled cylinders.

5.2 Simulations of the unsteady flow

For the unsteady periodic flow Re=100 is taken for the numerical validation and comparison with numerical results from other publications [27, 29, 36]. The characteristic quantities that were compared are the drag C_D and lift coefficient C_L, which were computed by (3.46-3.47), and the Strouhal number St. The dimensionless frequency, known as the Strouhal number, is given by $St = \frac{fd}{U}$, where D is the cylinder diameter and U is the freestream velocity. The parameter f is the frequency of the vortex shedding. To measure this quantity the values of the x-velocity at a point downstream of the cylinder at each time iteration were used. The easiest way, to compute the frequency f is to use the time between peaks of the x-velocity. An alternative way is to use a Fast Fourier Transform (FFT) of the x-velocity data over a given number of iterations, which easily can be done in Matlab.

The evolution of the flow past a smooth cylinder at $Re = 100$ is presented on fig.

	C_D	C_L	St
Ramšak et al. [40]			
N(bound. elem.)=112.500	1.286	0.149	0.168
Pacheco et al. [36]	1.41	-	0.167
Kim and Choi [27]	1.336	0.233	-
Stålberg et al. [29]	1.32	0.33	-
Present study	1.3373	0.215	0.1639

Table 5.2: Numerical result for the lift and drag coefficients and Strouhal number at $Re = 100$

5.15-5.14. The grid size here is 41×60 and the time step is 0.02. If we take too small time step periodical flow oscillations get dumped, the same behavior of the flow is mentioned in [40].

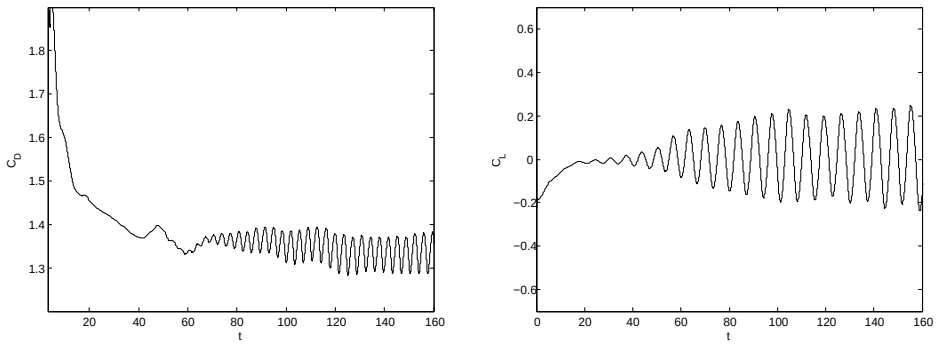

Figure 5.13: Drag (left) and lift (right) coefficients for the flow past smooth cylinder at Re=100

In the unsteady case the flow is non-uniform at large distances from the cylinder and has a complex structure. Hence to simulate this flow the grid should be more dense, than in the steady case. The smallest grid used in spectral discretization of the cylinder flow problem in literature is 81×100 [33]. In our tests we used grids with sizes from 41×40 to 61×60.

Now we present some flow simulations for dimpled cylinders. A flow past cylinders

t=188:

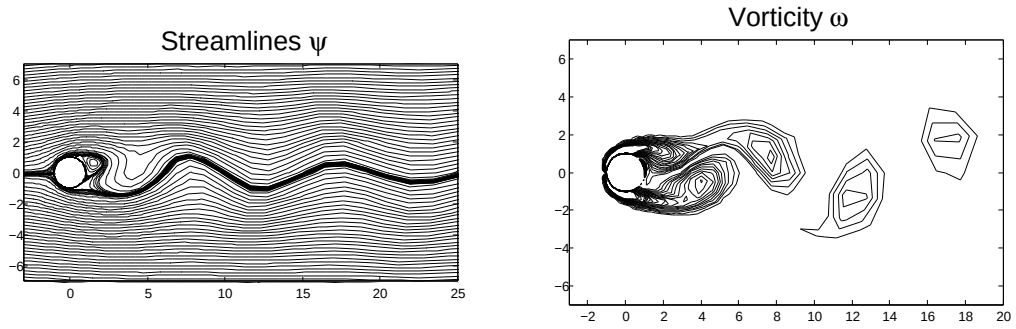

t=190:

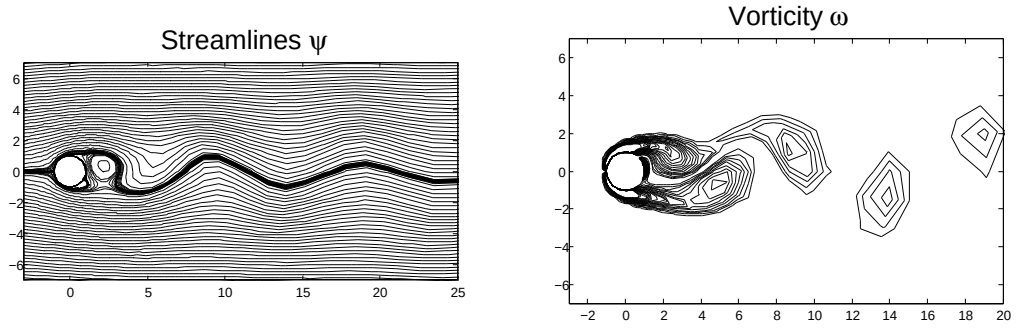

t=192:

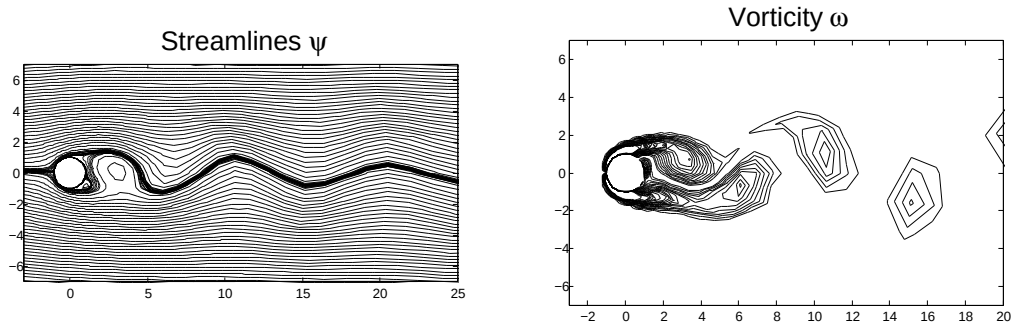

Figure 5.14: Evolution of the flow past smooth cylinder at Re=100

t=194:

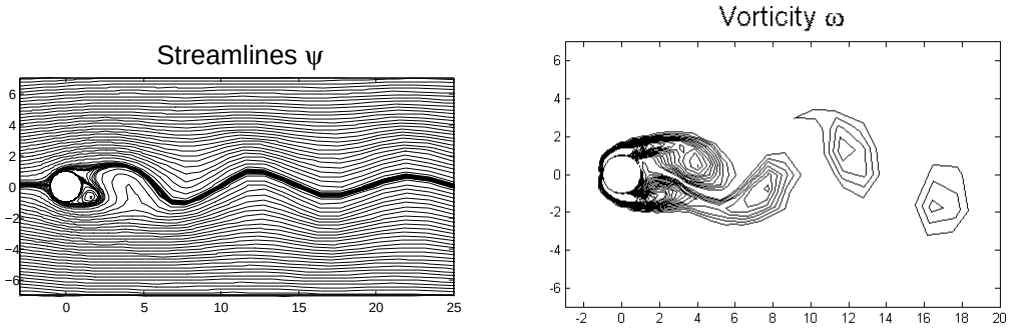

t=196:

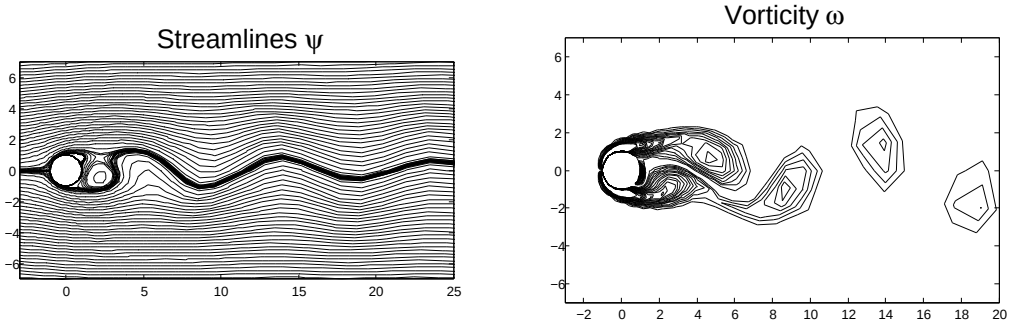

t=198:

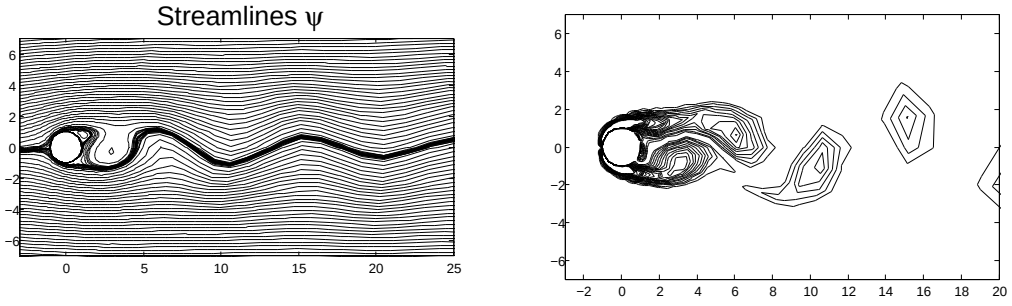

Figure 5.15: Evolution of the flow past smooth cylinder at Re=100(continue)

with 4 and 12 dimples were considered. The size of dimples ϵ was computed fromthe relation $\epsilon = \pi/c^2$, where c in the number of dimples. The grid size was 51×48. The flow at $Re = 45$ was simulated for the cylinder with 4 dimples (see fig. 5.17 and 5.16), and at $Re = 50$ for the cylinder with 12 dimples.

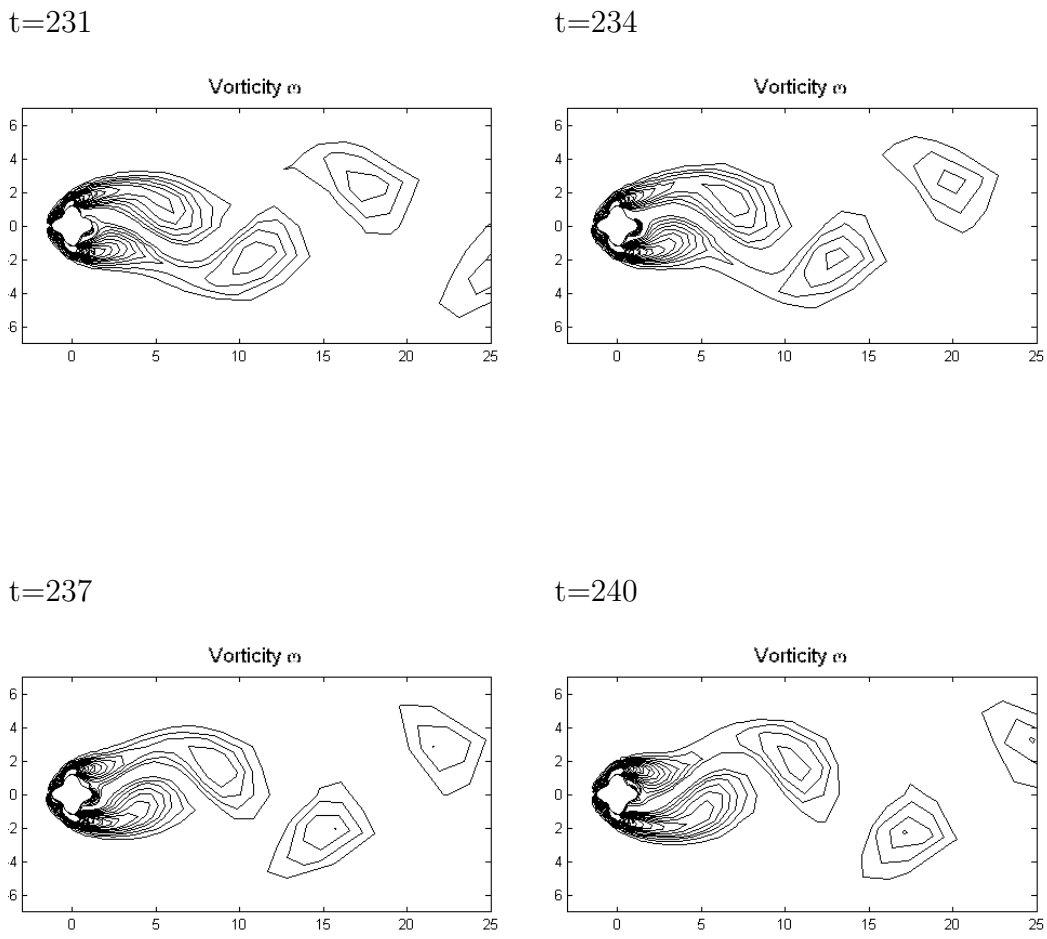

Figure 5.16: Evolution of the flow past a cylinder with 4 dimples at Re=45: vorticity.

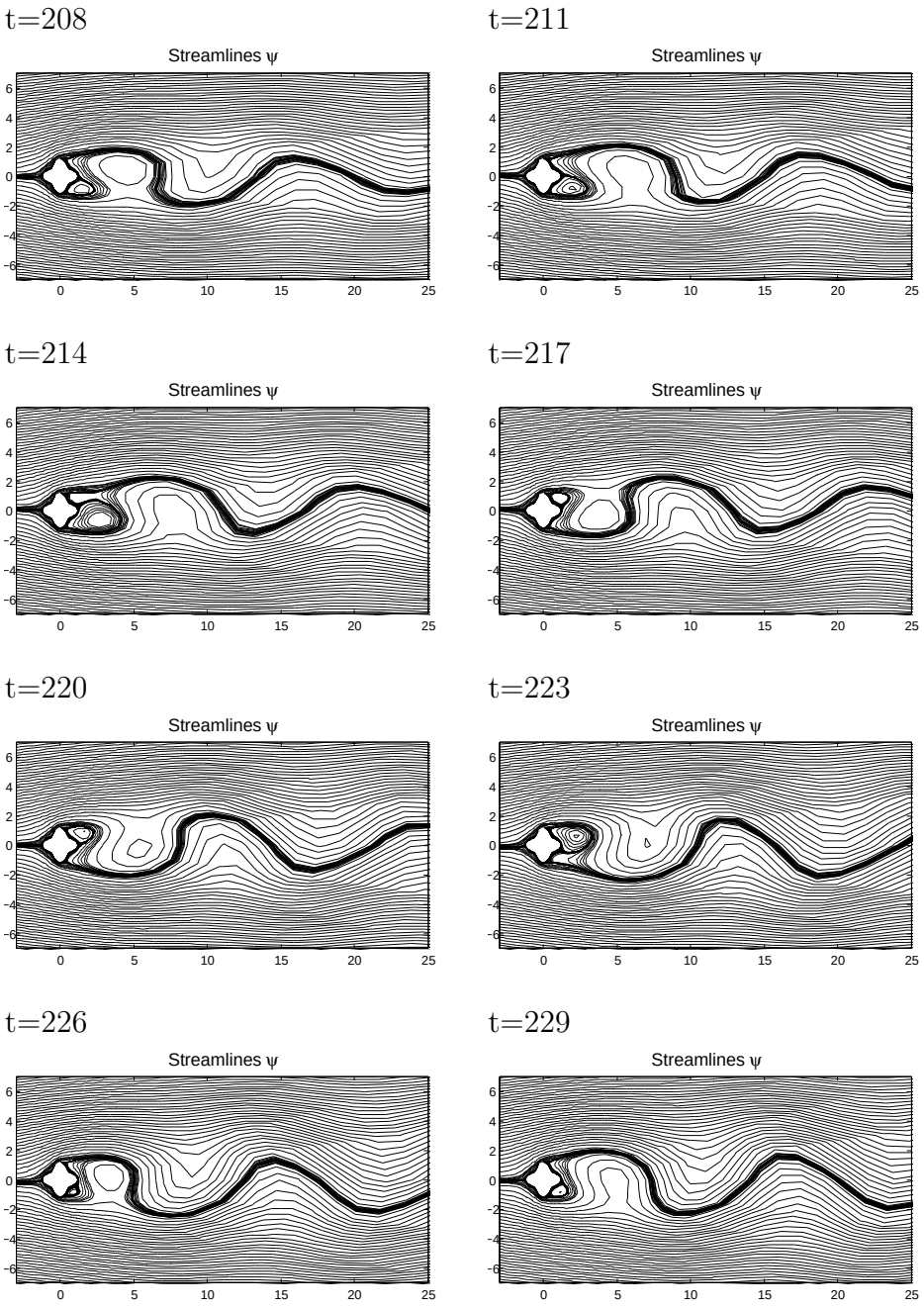

Figure 5.17: Evolution of the flow past a cylinder with 4 dimples at Re=45: stream-function.

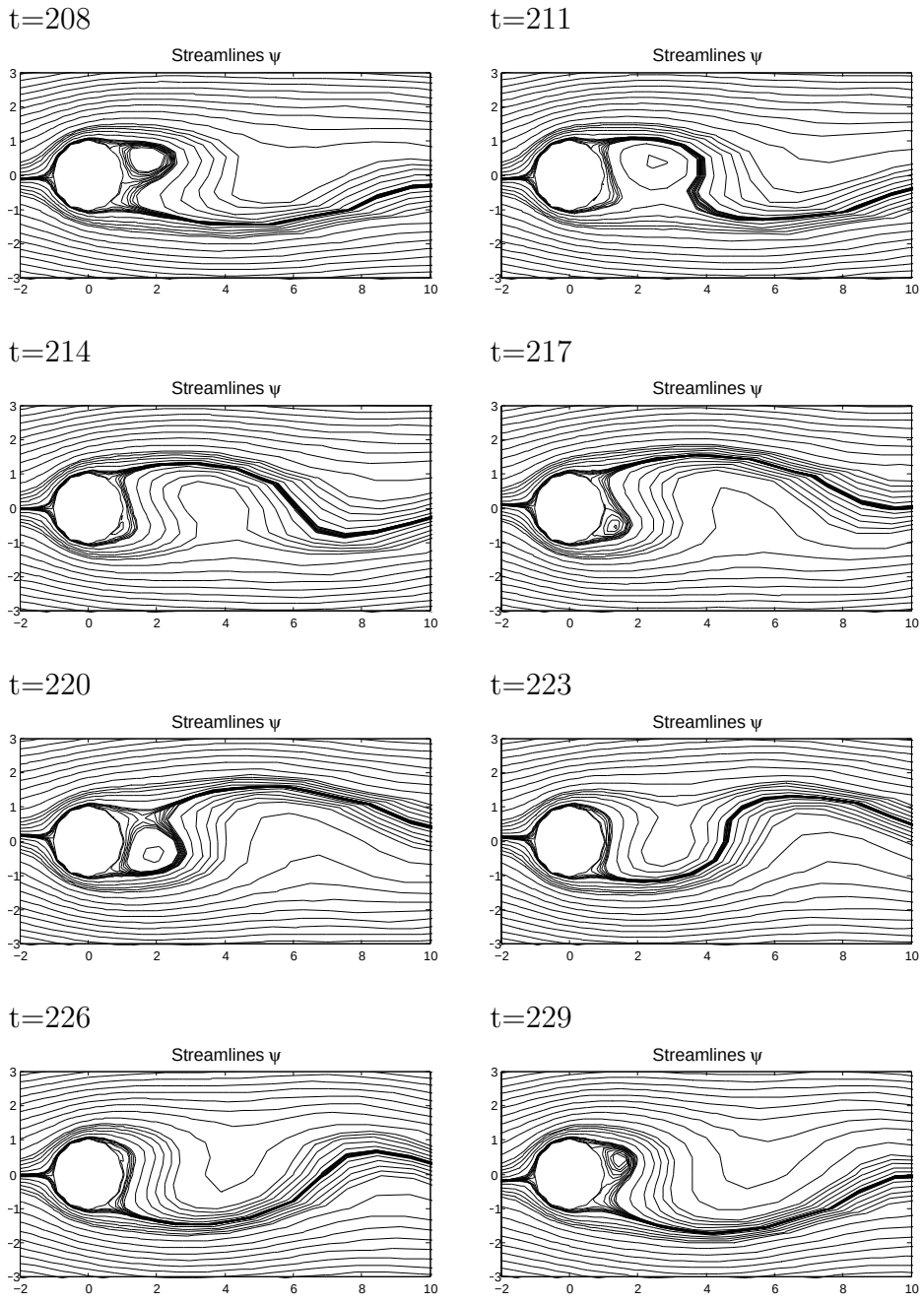

Figure 5.18: Evolution of the flow past a cylinder with 12 dimples at Re=50: stream-function.

Chapter 6

Conclusions and future work

The contributions of this thesis are the following:

- The highly accurate pseudospectral method was applied to the external flow problem with irregular semi-infinite geometry. The collocation grid was defined on the unit disk using Fourier nodes in angular direction and Chebyshev nodes in radial direction. To solve the problem the transformation from the unit disk to the irregular semi-infinite domain was presented.

- The problem of flow past a dimpled cylinder was formulated on the semi-infinite domain instead of using truncated domain [33, 36, 40]. As a result we avoided the problem of choosing the size of the domain around a cylinder and formulating outer boundary conditions. High order method like pseudospectral methods are very sensitive to the accuracy of farfield boundary conditions and the distance of the farfield boundary from the body. Hence solving the problem on the entire semi-infinite region plays an important role in the accuracy of the solution.

- In this thesis we proposed the method which has a certain geometrical flexibility. Different shapes of cylinders can be taken by varying the boundary function $\gamma(\theta)$ as long as it is symmetric with respect to the origin.

- Also our method has certain flexibility in defining an outer collocation grid.

Coordinate transformations are written in general form using metric tensor components. The distribution of outer collocation nodes in radial direction cab by varied by changing the map $f(R) : [0, 1] \to [1, \infty]$. It was found in this project that proper definition of the function $f(R)$ plays an essential role in the solution of the problem. After carrying out many numerical experiment with different functions $f(R)$ it was noticed that the best were obtained when the function of the form $1 - aln(R) - b(1 - R)$ was used. This function provides a mesh which is nearly uniform in a region close to a cylinder (the area of $\approx b$ radiuses of a cylinder) and sparse enough far from the body. Hence the mesh has a good resolution in a region with vortices and yet takes into account the flow far from a cylinder. We don't claim that it is the very best choice, but result of experiment with this function showed good agreement with other authors.

The steady solver has been validated by computing flow past a smooth cylinder and good agreement of characteristic parameters, like wake length, separation angle and drag coefficient is obtained with established experimental and numerical results [9, 11, 13, 36, 40, 45, 48]. Furthermore, the spectral accuracy has been shown in both angular and radial directions.

The unsteady solver has been tested by computing the Strouhal number, drag and lift coefficients for a flow past a smooth cylinder, and showed good agreement with results in [27, 29, 36, 40].

The following future work can be done as a continuation of this project:

- A better research and analysis in defining the outer grid and the function $f(R)$

can be done.

- Further improvement of the presented method can be done by defining an uneven distribution of angular nodes. Then we can get finer grid for the region behind a cylinder, then for the front area. One way of defining an uneven distribution for periodic problems is to use arctan / tan map suggested by Boyd [4]. For a function that is periodic in θ with period 2π such map has a form:

$$\xi(\theta) = 2 \arctan\left(K \tan\frac{\theta}{2}\right), \qquad \theta \in [-\pi, \pi]$$

  here K is a stretching parameter. If we take evenly spaced θ_k, then $\xi(\theta_k)$ will give us an unevenly spaced grid points with clustering near 0. Hence we can get finer grid behind a cylinder, where flow has a complex structure, and coarser grid elsewhere. We believe, that this should improve the efficiency of the present method in term of memory, because the total number of grid points, required to get an accurate result will be smaller.

- Presented method for the steady flow simulations can be used to find critical Reynolds number at which symmetric steady flow becomes periodic. It is well known that transition to periodic behavior as Re varies corresponds to a Hopf bifurcation where a complex pair of eigenvalues of the Jacobian matrix of the Navier-Stokes equations crosses the imaginary axis. This problem was studied using low order method, for example Jackson in [25] determined critical Re for the smooth cylinder using FEM. The critical Reynolds number for dimpled cylinder of various shapes and convergence of Re_c with the number of collocation point can be studied.

- It is also important to address the problem of stability of the unsteady solution for the flow past dimpled cylinders.
- Flow past rotating cylinder with dimples can be simulated.
- Simulation for large $Re > 200$ can be studied. In this case three-dimensional model has to be considered [54].

This work shows that using global approximation methods over an entire domain is very expensive in terms of CPU time and computer memory. As an alternative to get high order approximations of PDEs either spectral element [4, 37, 49] or spectral volume method [52] can be employed. These methods are based on unstructured grids with curvilinear elements, where spectral approximations are used on each element. These methods are geometrically flexible and approximation matrices are sparse with full blocks, which correspond to spectral elements. This work is an important step for the further research in high order methods for problems with complex geometry.

Bibliography

[1] Elmar Achenbach. Influence of the surface roughness on the cross-flow around a circular cylinder. *J. Fluid Mech.*, 46:321 – 335, 1971.

[2] F. Auteri, L. Quartapelle, and L. Vigevano. Accurate $\omega - \psi$ spectral solution of the singular driven cavity problem. *J. Comput. Phys.*, 180:597–615, 2002.

[3] P.W. Bearman and J.K. Harvey. Control of circular cylinder flow by the use of dimples. *AIAA*, 31(10):1753–1756, 1993.

[4] John P. Boyd. *Chebyshev and Fourier spectral methods.* DOVER Publications, 2nd edition, 2000.

[5] Heli Chen, Yuhong Su, and Bernie Shizgal. A direct spectral collocation poisson solver in polar and cylindrical coordinates. *J. Comput. Phys.*, 160:453–469, 2000.

[6] Mo-Hong Chou. A multigrid pseudospectral method for steady flow computation. *Int. J. Numer. Meth. Fluids*, 43:25–42, 2003.

[7] H. J. H. Clercx. A spectral solver for the navierstokes equations in the velocity-vorticity formulation for flows with two nonperiodic directions. *J. Comput. Phys.*, 137:186–211, 1997.

[8] Roque Corral and Javier Jimenez. Fourier/chebyshev methods for the incompressible navier-stokes equations in infinite domains. *J. Comput. Phys.*, 121:261–270, 1995.

[9] M. Coutanceau and R. Bouard. Experimental determination of the main features of the viscous flow in the wake of a circular cylinder in uniform translation: steady flow. *J. Fluid Mech.*, 79:231, 1977.

[10] P. Demaret and M. O. Deville. Chebyshev pseudospectral solution of the stokes equations using finite element preconditioning. *J. Comput. Phys.*, 83:463–484, 1989.

[11] S. C. R. Dennis and G. Z. Chang. Numerical solutions for steady flow past a circular cylinder at reynolds numbers up to 100. *J. Fluid Mech.*, 42:471–490, 1970.

[12] M. O. Deville, P. F. Fischer, and E. H. Mund. *High–Order methods for incompressible fluid flow*, volume 9 of *Cambridge monographs on applied and computational mathematics*. Cambridge University Press, 2002.

[13] B. Fornberg. A numerical study of steady viscous flow past a circular cylinder. *J. Fluid Mech.*, 98:819–855, 1980.

[14] Bengt Fornberg. *A practical guide to pseudospectral methods*, volume 1 of *Cambridge monographs on applied and computational mathematics*. Cambridge University Press, 1996.

[15] Robert W. Fox and Alan T. McDonald. *Introduction to fluid mechanics*. John Wiley & Sons, Inc., fourth edition, 1994.

[16] Daniele Funaro. *Polynomial approximation of differential equations*. Lecture

notes in physics. New series m. Monorgaphs; m8. Berlin ; New York : Springer-Verlag, 1992.

[17] Daniele Funaro and Wilhelm Heinrichs. Some results about the pseudospectral approximation of one-dimensional fourth-order problems. *Numer. Math.*, 58:399–418, 1990.

[18] David Gottlieb and Steven A. Orszag. *Numerical analysis of spectral methods: theory and application.* Regional conference series in applied mathematics. SIAM, 1977.

[19] Wilhelm Heinrichs. Stabilization techniques for spectral methods. *J. Sci. Comput.*, 6(1), 1991.

[20] Wilhelm Heinrichs. A spectral multigrid methods for the stokes problem in streamfunction formulation. *J. Comput. Phys.*, 102:310–318, 1992.

[21] Wilhelm Heinrichs. Spectral collocation schemes on the unit disc. *J. Comput. Phys.*, 199:66–86, 2004.

[22] W. Huang and D. M. Sloan. Pole condition for singular problems: The pseudospectral approximation. *J. Comput. Phys.*, 107:254–261, 1993.

[23] Weizhang Huang and Tao Tang. Pseudospectral solutions for steady motion of a viscous fluid inside a circular boundary. *Appl. Numer. Math.*, 33:167–173, 2000.

[24] jr. J. E. Dennis and Robert B. Schnabel. *Numerical methods for unconstrained optimization and nonlinear equations.* Prentice-Hall series in computational

mathematics. Prentice-Hall,Inc., Englewood Cliffs, New Jersey 07632, 1983.

[25] C. P. Jackson. A finite–element study of the onset of vortex shedding in flow past various shaped bodies. *J. Fluid Mech.*, 182:23–45, 1987.

[26] Andreas Karageorghis and Tao Tang. A spectral domain decomposition approach for steady navier-stokes problems in circular geometries. *Comp. Fluids*, 25(6):541–549, 1996.

[27] Jinsung Kim and Haecheon Choi. Distributed forsing of flow over a circular cylinder. *Physics of Fluids*, 17, 2005.

[28] L. Kleiser and U. Schumann. Treatment of incompressibility and boundary conditions in 3-d numerical spectral simulations of plane channels flows. In E.H. Hirschel, editor, *Proc. 3rd GAMM Conf. Numerical Methods in Fluid Mechanics, Notes on Numerical Fluid Mechanics 2*, page 165. Vieweg,Braunschweig, 1980.

[29] Erik Stålberg, Arnim Brüger, Per Lötstedt, Arne V. Johansson, and Dan S. Henningson. High order accurate solution of flow past a circular cylinder. *J. Sci. Comput.*, 27:431–441, 2006.

[30] J. M. Lopez, F. Marques, and Jie Shen. An efficient spectral-projection method for the navier-stokes equations in cylindrical geometries. *J. Comput. Phys.*, 176:384–401, 2002.

[31] M. Manna and A. Vaccay. An efficient method for the solution of the incompressible navier-stokes equations in cylindrical geometries. *J. Comput. Phys.*,

151:563–584, 1999.

[32] Rabindra D. Mehta. Aerodynamics of sports balls. *Ann. Rev. Fluid Mech.*, 17:151–189, 1985.

[33] R. Mittal and S. Balachandar. Direct numerical simulation of flow past elliptic cylinders. *J. Comput. Phys.*, 124:351–367, 1996.

[34] Rajat Mittal. A fourier-chebyshev spectral collocation method for simulating flow past spheres and spherois. *Int. J. Numer. Meth. Fluids*, 30:921–937, 1999.

[35] S. A. Orszag. Spectral methods for problems in complex geometries. *J. Comput. Phys.*, 37:70–92, 1980.

[36] J. R. Pacheco, A. Pacheco-Vega, T. Rodić, and R. E. Peck. Numerical simulations of heat transfer and fluid flow problems using an immersed-boundary finite-volume method on nonstaggered grids. *Numerical Heat Transfer*, 48:1–24, 2005.

[37] Roger Peyret. *Spectral methods for incompressible viscous flow*, volume 148 of *Appl. Math. Sci.* Springer, 2002.

[38] Timothy N. Phillips and Alaeddin Malek. Multidomain collocation methods for the stream function formulation of the navier-stokes equations. *SIAM J. Sci. Comput.*, 16(4):773–797, 1995.

[39] V. G. Priymak and T. Miyazakiy. Accurate navierstokes investigation of transitional and turbulent flows in a circular pipe. *J. Comput. Phys.*, 142:370–411, 1998.

[40] Matjaž Ramšak, Leopold Škerget, Matjaž Hriberšek, and Zoran Žunič. A multidomain boundary element method for unsteady laminar flow using stream functionvorticity equations. *Engineering Analysis with Boundary Elements*, 29:1–14, 2005.

[41] Isabelle Raspo. A direct spectral domain decomposition method for the computation of rotating flows in a t-shape geometry. *Computers & Fluids*, 32:431–456, 2003.

[42] Yousef Saad. *Iterative methods for sparse linear systems*. SIAM, 2nd edition, 2003.

[43] W. W. Schultz, N. Y. Lee, and J. P. Boyd. Chebyshev pseudospectral method of viscous flows with corner singularities. *J. Sci. Comput.*, 4(1), 1989.

[44] Jie Shen. A new fast chebyshev-fourier algorithm for poisson-type equations in polar geometries. *Appl. Numer. Math.*, 33:183–190, 2000.

[45] H. Takami and H.B. Keller. Steady two-dimensional viscous flow of an incompressible fluid past a circular cylinder. *Phys. Fluids Suppl.*, 12:11–51, 1969.

[46] D. J. Torres and E. A. Coutsias. Pseudospectral solution of the two–dimentional navier–stokes equations in a disk. *SIAM J. Sci. Comput.*, 21(1):378–403, 1999.

[47] L. N. Trefethen. *Spectral Methods in Matlab*. SIAM, 2000.

[48] D. J. Tritton. Experiments on the flow past a circular cylinder at low reynolds number. *J. Fluid Mech.*, 6:547–567, 1959.

[49] James Trujillo and George Em Karniadakis. A penalty method for the vorticity-velocity formulation. *J. Comput. Phys.*, 149:32–58, 1999.

[50] J. M. Vanel, R. Peyret, , and P. Bontoux. A pseudo-spectral solution of vorticity-stream function equations using the influence matrix technique. In K. W. Morton, editor, *Numerical Methods for Fluid Dynamics II*, page 463. Oxford Univ. Press,Oxford, 1986.

[51] Robert G. Voigt, David Gottlieb, and M. Yousuff Hussaini. *Spectral methods for partial differential equations*. SIAM, 1984.

[52] Z. J. Wang. Spectral (finite) volume method for conservation laws on unstructured grids. *J. Comp. Phys.*, 178:210–251, 2002.

[53] J. A. C. Weideman. Numerical integration of periodic functions: A few examples. *The American Mathematical Monthly*, 109(1):21–36, 2002.

[54] C. H. K. Williamson. Vortex dynamics in the cylinder wake. *Annu. Rev. Fluid. Mech.*, 28:477–539, 1996.

[55] Chuanju Xua and Richard Pasquetti. On the efficiency of semi-implicit and semi-lagrangian spectral methods for the calculation of incompressible flows. *Int. J. Numer. Meth. Fluids*, 35:319–340, 2001.

[56] Z. Yin, Li Yuan, and Tao Tang. A new parallel strategy for two-dimensional incompressible flow simulations using pseudo-spectral methods. *J. Comput. Phys.*, 210:325–341, 2005.